June 1997 ANL-NT-39

STATUS REPORT ON SEVERE ACCIDENT MATERIAL PROPERTY MEASUREMENTS

by

M. T. Farmer, L. McUmber, R. W. Aeschlimann, and B. W. Spencer

Reactor Engineering Division
Argonne National Laboratory
9700 South Cass Avenue
Argonne, IL 60439

NT TECHNICAL MEMORANDUM NO. 39

Results reported in the NT-TM series of memoranda frequently are preliminary and subject to revision. Consequently, they should not be quoted or referenced without the author's permission.

TABLE OF CONTENTS

LIST OF FIGURES

LIST OF FIGURES
(Contd.)

LIST OF TABLES

STATUS REPORT ON SEVERE ACCIDENT MATERIAL PROPERTY MEASUREMENTS

by

M. T. Farmer, L. McUmber, R. Aeschlimann, and B. W. Spencer

ABSTRACT

Under the sponsorship of the International Nuclear Safety Center (INSC) at Argonne National Laboratory, measurements of selected material properties of molten reactor core material (corium) were made. The corium used in the measurements was a mixture of UO_2, ZrO_2 and Zr, with the oxygen content being a parameter to reflect different stages of zirconium oxidation. The mixtures that were used were representative of typical in-vessel melt sequences. For most of the measurements, the UO_2/ZrO_2 mass ratio was 1.51, which is representative of VVER/440 melt compositions as well as the melt composition for most US BWRs.

Measurements were made of the solidus/liquidus temperatures of various corium compositions by using a Differential Thermal Analysis technique. An observation on the solubility of unoxidized Zr in the oxide phase was made by metallographic analysis of solidus/liquidus melt samples. The results of laminar flow corium spreading tests in one dimension were used to estimate the viscosity of various corium compositions. Measured solidus and liquidus temperatures for compositions representative of Zr oxidation of 30, 50 and 70 percent were compared with those obtained from a phase diagram provided by Kurchatov Institute. It was found that the experimental measurements agreed well with the phase diagram values at 70 percent oxidation, but the measured solidus temperatures were higher than those on the phase diagram and the measured liquidus temperatures were lower than those on the phase diagram at 30 and 50 percent oxidation. From a microstructure examination it was determined that there was no global segregation into distinct metal and oxide phases during the cooldown of a sample in which there was initially 70 percent Zr oxidation. Therefore it is concluded that Zr metal is soluble in the oxide phase under molten conditions. Viscosity estimates were made for compositions representative of Zr oxidation of 30, 50 and 70 percent by fitting the results of spreading tests to Huppert's equation. It was found that, at a temperature of 2500 C, the viscosity varied by three orders of magnitude over this range of compositions.

1.0 INTRODUCTION

A series of experiments has been conducted at Argonne National Laboratory to investigate selected material properties of molten reactor core material (corium). The corium in these experiments consisted of mixtures of $(U,Zr)O_{2-x}$, with the oxygen content of the mixture varied to reflect various stages of zirconium oxidation. The melts are representative of typical in-vessel core melt sequences (i.e., concrete oxides, which arise during postulated accident sequences in which the reactor pressure vessel is breached leading to melt interaction with the containment basemat, were not included in this work). Specific core compositions addressed in this study are shown in Table 1. For most of the tests conducted, the UO_2/ZrO_2 mass ratio was fixed at 1.51, which is representative of VVER/440 melt compositions as well as the melt composition for most US BWRs. The purpose of this report is to summarize the status of these experimental efforts.

Table 1. Summary of Target Corium Compositions Considered in this Study

Constituent	wt %				
	0% Zr Oxidation	30% Zr Oxidation	50% Zr Oxidation	70% Zr Oxidation	100% Zr Oxidation
UO_2	67.2	64.9	63.5	62.2	60.3
ZrO_2	0	12.9	20.9	28.7	39.7
Zr	32.8	22.2	15.6	9.1	0

The specific objectives of the experiments are as follows:

i) Measure the solidus/liquidus temperatures of various corium compositions,

ii) Measure the solubility of unoxidized Zr in the oxide phase,

iii) Estimate the viscosity of various compositions.

Two experiment facilities were constructed in order to carry out these measurements. The first facility was centered on use of a commercial graphite resistance furnace capable of sustained operations at up to 2800 C (3073 K). This facility was used to measure the melt solidus/liquidus using the standard Differential Thermal Analysis[1] technique. Zirconium solubility was determined following these experiments by sectioning the samples and performing metallographic analysis. The second facility consisted of a one dimensional (3 m long by 15 cm wide) spreading channel. Core melts were generated using exothermic chemical reactions. Spreading was initiated using a "dam break" approach (i.e., spreading was initiated following meltout of a thin stainless steel barrier). The leading edge penetration as a function of time was measured. Based on the spreading rate, the corresponding corium viscosity was determined from well known analytical solutions[2] which relate spreading rate to initial melt mass, channel width, and viscosity for viscous flows.

The structure of this report is as follows. The experiment facility for measurement of corium liquidus/solidus and Zr solubility is described first. The experiment results from this series of tests is then described. The facility for determination of viscosity is then described, followed by a presentation of the experiment results. Recommendations for future experiments are made at the end of each section.

2.0 LIQUIDUS/SOLIDUS AND Zr SOLUBILITY MEASUREMENT

2.1 Facility Description

The experiment setup for the liquidus/solidus temperature and Zr solubility measurements is shown in Figure 1. The samples were heated in a 20 kVA, water cooled, SCR-controlled, graphite resistance furnace made by Astro, Inc. The furnace has a maximum sustained operating temperature of 2800 C; the hot zone of the furnace measures 7.6 cm in diameter by 15.2 cm high. The maximum axial temperature gradient across the furnace hot zone is 6 C, which ensures uniform heating of both the sample and reference crucibles during the experiments. For the initial test series, the crucible material for containing the melts was chosen to be ZrC, based on experience from the Russian Academy of Science.[3] These ZrC crucibles were obtained from Cerac, Inc. in Milwaukee, Wisconsin. The crucibles used in these tests measured 25.4 mm OD and were 25.4 mm high; the crucible wall/base thickness was constant at 2.38 mm. Typical crucible material purity was 99.5%, with Hafnium being the principal impurity.

As shown in Figure 1, both the sample and reference crucibles were held in a graphite fixture. The crucible containing the melt was placed in the top of the fixture, while the reference crucible was symmetrically mounted in the bottom of the fixture. The reference crucible was used for controlling the furnace temperature. Due to the high temperatures required to conduct these tests (up to 2750 C), pyrometry was required for reliable temperature measurements. Both the melt and reference crucible temperatures were measured using Ircon two-color pyrometers with operating temperature ranges of 1500-3500 C. Both pyrometers were calibrated by the manufacturer using standards traceable to NIST. The standard error in the temperature measurement is 1% over the operating range for these devices. (Note: this error is identical to the standard error for Type C, W5%Re/W26%Re, thermocouples).[4] The pyrometers were focused on the melt and reference crucible surfaces through quartz window viewports located at the top and bottom of the furnace, respectively. Both viewports were purged with helium gas (2 slpm total flowrate) during the experiment to prevent aerosol deposition on the viewport windows. As shown in Figure 1, both crucibles were covered with heat shields containing 6.4 mm diameter holes in the center of the shields. The pyrometery measurements were made by viewing the target surfaces through these holes. Aside from minimizing radiation heat losses, the small openings which the shields provide

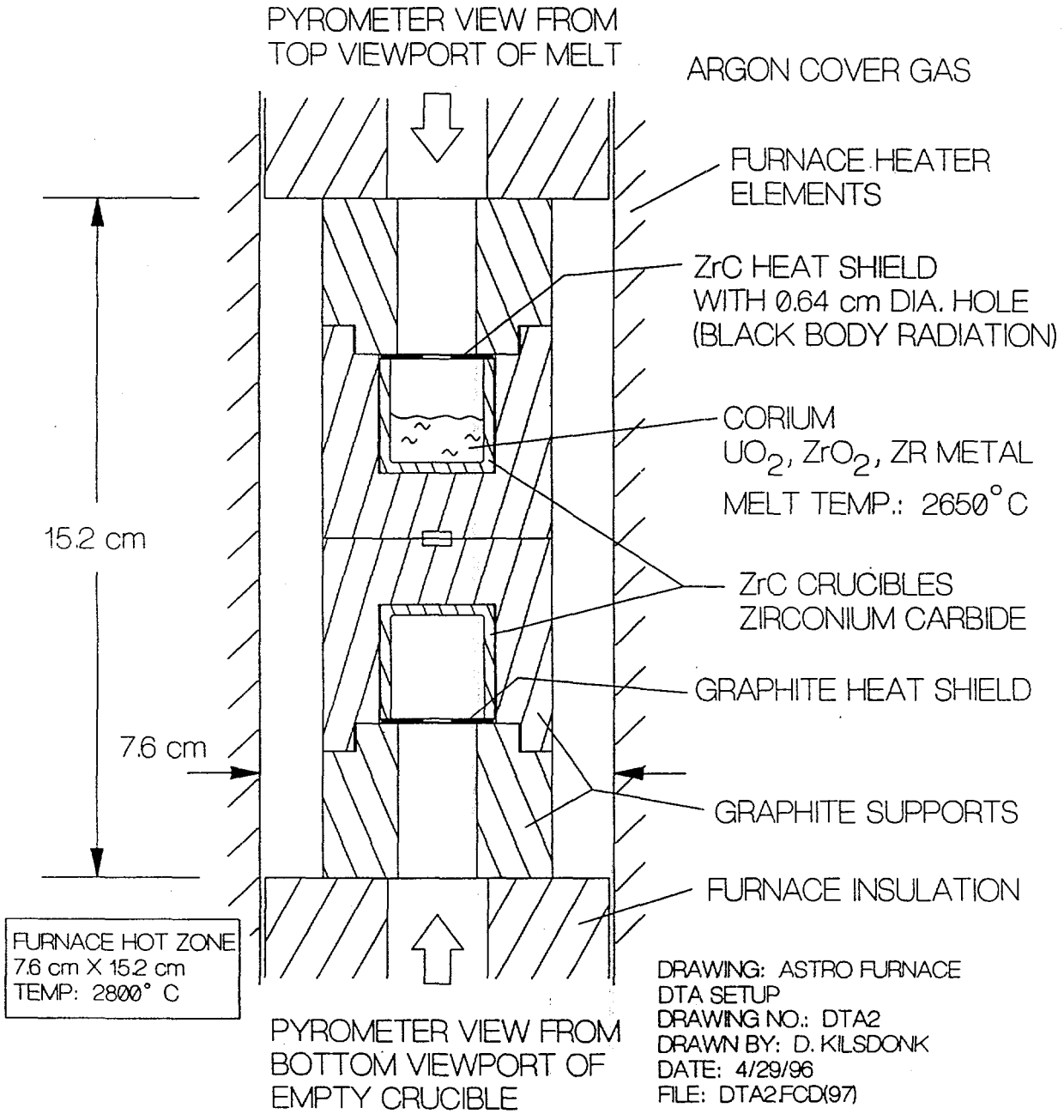

Figure 1. Illustration of Experiment Apparatus for Liquidus/Solidus Temperature Measurements

allows the assumption of black body radiation to be made. As a result, the emissivity of the crucible material and the melt do not need to be known to ensure reliable measurements. Heatup of the melt and reference crucibles was controlled by a Eurotherm Model 902P programmable controller. The control signal was taken from the lower pyrometer focused on the reference crucible surface. Linear heating/cooling ramps in the range of 10-25 C/minute were used in these tests to measure the solidus/liquidus temperatures.

The initial core compositions used in these tests were made by uniformly blending appropriate proportions of UO_2 (depleted), ZrO_2, and Zr powders in a glass jar before placing the chemical mixture into the crucible. Chemical analyses of the materials used in these experiments is provided in Tables 2-4. The UO_2 analysis was performed by the Analytical Chemistry Laboratory at Argonne, while the Zr and ZrO_2 analyses were supplied by the manufacturer (Johnson Matthey Alfa Aesar and Cerac Inc., respectively). The UO_2 and ZrO_2 powders are 99.95% + purity, while the Zr purity is 99.8%. The principal impurity in the Zr is iron (0.14%). The particle size of the UO_2 and ZrO_2 powders was < 45 μm (-325 Mesh), while the particle size of the Zr was in the range 300-600 μm (-30 + 50 Mesh).

Various cladding oxidation states were simulated by introducing the appropriate proportions of Zr/ ZrO_2 powders into the mixture. To ensure that the oxygen potential was preserved to the greatest extent possible over the course of the experiments, the furnace was evacuated to 10 Pascal (10^{-4} atmospheres) and then backfilled with high purity (99.995%) helium before starting each test.

The general operating procedure for the experiments was as follows. After the powders were loaded into the test crucible and the crucible was installed in the graphite fixture, the furnace was inerted with helium using the above procedure. The sample was then manually heated to 1600 C (i.e., slightly above lower temperature limit of 1500 C for the pyrometers). At this point, the furnace was placed in automatic control mode in which the samples were heated at a constant rate based on feedback from the pyrometer measuring the reference crucible temperature. For most tests, the samples were put through two heating and cooling cycles to look for repeatability in any observed peaks or inflection points in the differential temperature traces. Generally, the samples were heated at a constant rate of 25 C/minute to a temperature of 2700 C, followed by a 5 minute hold at this temperature. The samples were then cooled at a constant rate of 10 C/minute to 1700 C. After 1700 C

Table 2. Impurities in UO_2 Powder Used in DTA Tests

Element	Concentration, µg/g
Al	37
Ba	<3
Be	<1
Ca	6
Cd	<1
Co	<3
Cr	2
Cu	3
Fe	14
K	<30
Li	<3
Mg	2
Mn	<1
Mo	<6
Na	69
Ni	<2
Pb	<10
Sr	<1
Ta	<0.1
Ti	<2
V	<2
W	<0.2
Zn	86
Zr	<1
	<285.3

Table 3. Impurities in ZrO_2 Powders Used in DTA Tests

Element	Concentration (wt%)
Ca	< 0.001
Cu	< 0.001
Si	0.008
Ti	0.008

Table 4. Summary of Principal Impurities for Zr Powder Used in DTA Tests

Element*	Concentration (wt%)
Al	0.008
Fe	0.139
Mg	0.022
Ti	0.005
Total	0.174

* A total of 69 elements were measured. All other elements not shown in this table are present at a level of <0.001 wt %.

was reached, the samples were reheated to 2700 C at a rate of 10 C/minute. After 2700 C was reached for the second time, the furnace power was turned off and the samples were cooled as rapidly as possible to room temperature using the water cooling circuits in the furnace. The rapid cooling scheme was employed to preserve the various phases which were present in the fully molten state for later posttest examination. The typical sample cooling rate after the furnace power was turned off was 250 C/minute. More detail regarding the experiment operating procedure is given below in the discussion of test results.

2.2 Test Results

As summarized in Table 5, a total of four tests were conducted in the experiment series. Three tests were conducted with corium spanning the range of 30-70% Zr oxidation states. The fourth test was conducted with 100% Zr to check the experiment technique. Corium masses were in the range 17.37-18.39 g. The Zr calibration test was conducted with 13.6 g of material.

The first test in the experiment series (Test No. 1) utilized 70% oxidized corium. The sample and reference temperatures as a function of time for this test are shown in Figure 2, while the temperature difference between the reference and sample as a function of the reference temperature is shown in Figure 3. The thermal cycle for this test consisted of a 10 C/min. heatup to 2700 C. At this point, the furnace power was turned off and the sample was cooled to room temperature. As is evident from Figure 3, the first endothermic break in the differential temperature curve occurs at 2000 C during the heatup, indicating onset of melting in the sample. A similar (exothermic) inflection point is observed at the same temperature upon cooling of the sample. The estimated error in this reading is ±30 C, which includes the standard error in the pyrometer reading, plus an additional 10 C uncertainty which is attributable to the fact that the pyrometer measures the surface temperature of the sample, as opposed to the center (or bulk) temperature[1]. The second break in the differential temperature trace begins at ~2400 C and terminates abruptly at ~2550 C where the differential temperature undergoes a steep temperature change of ~15 C. After the power was turned off, an exothermic peak is observed at 2600 C in the cooling trace. Based on this data, the liquidus temperature for this system was estimated to be 2600 C ±35 C. The discontinuous change in differential temperature observed during heatup of the sample at ~2550 C is most likely attributable to a color change in the material upon complete melting, which causes a shift in the pyrometer reading due to a change in intensity of the two monitored wavelengths of the sample. This observation is supported by the fact that the differential temperature trace showed no discontinuities

[1] The maximum 10 C differential temperature between the surface and center of the sample is estimated by solving the transient 1-D heat conduction equation in the axial direction for the sample. The upper and lower surface temperatures of the sample are assumed to ramp at a constant rate of 25 C/minute. The temperature distribution in the sample is calculated using the integral method assuming the distribution is symmetrical around the axial midplane of the sample. The melt depth is calculated to be 7.2 mm given the crucible dimensions, melt mass, and the assumed melt density of 7500 Kg/m^3. On this basis, the maximum temperature differential of 10 C is calculated assuming a melt thermal conductivity of 2 W/m·K and a melt specific heat of 600 J/Kg·K.

Table 5. Summary of DTA Tests

Test	Corium Composition (wt%)	Zr Oxidation (%)	Melt Mass (g)	Notes
1-C	100 Zr	N/A	13.61	Calibration Test; two heating/cooling cycles
3	64.9 UO_2, 20.9 ZrO_2, 22.2 Zr	30	17.600	Two heating/cooling cycles
2	63.5 UO_2, 20.9 ZrO_2, 15.6 Zr	50	17.369	Two heating/cooling cycles
1	62.2 UO_2, 28.7 ZrO_2, 9.1 Zr	70	18.391	Constant heating rate to 2700 C; power off

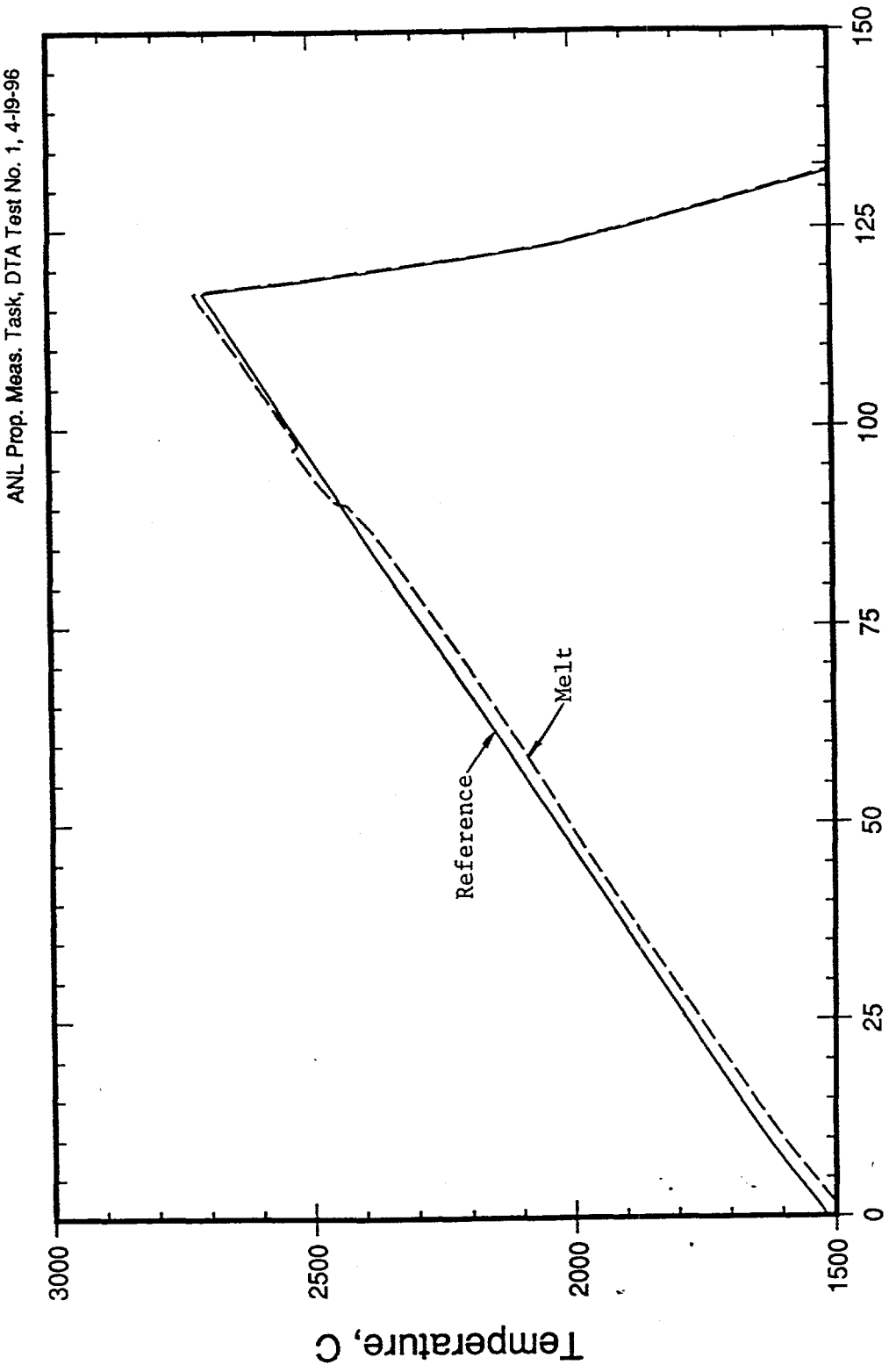

Figure 2. Melt and Reference Crucible Temperatures for Test No. 1 (70% Oxidized Corium)

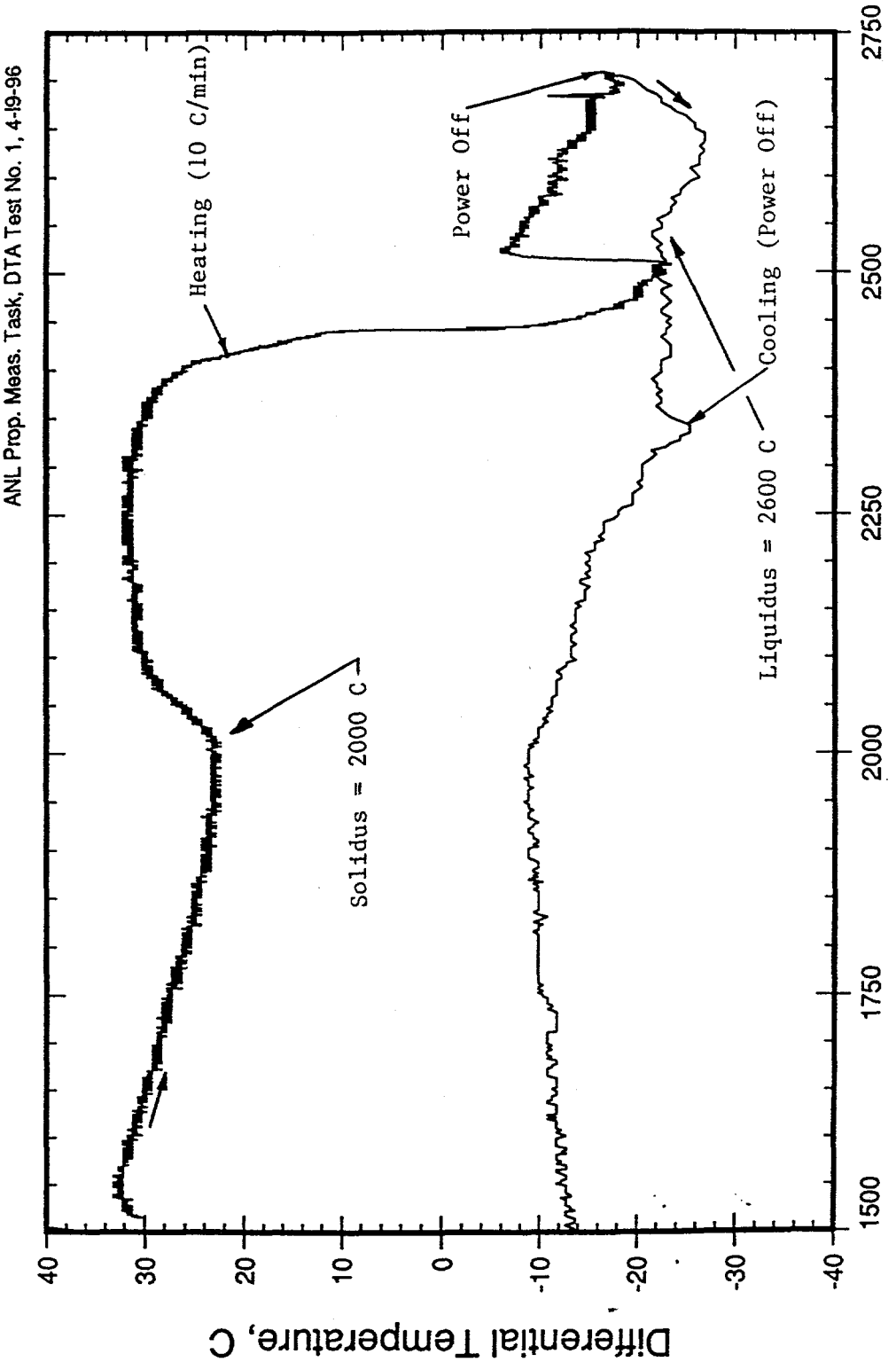

Figure 3. Temperature Difference Between Reference Crucible and Melt for Test No. 1 (70% Oxidized Corium)

upon cooling (i.e., after the sample had melted). As a result of this observation, the heating cycle for later tests was modified to include two heating and cooling cycles. In these later tests, the temperature discontinuity was never noted after initial complete melting of the material.

The second test (Test No. C-1) was conducted with pure Zr metal as a test of the experimental technique. As shown in Table 5, the powder mass corresponded to 13.61 g. The thermal cycle for the sample consisted of a 25 C/minute heatup to 2200 C (i.e., ~350 C above the reported Zr melting temperature of 1855 C), followed by a five minute hold at 2200 C. The sample was then cooled to 1600 C at a rate of 10 C/minute. After the sample was cooled to 1600 C, the sample was reheated to 2200 C at a rate of 10 C/minute. After 2200 C was reached the second time, the power was turned off to terminate the test. The sample and reference temperatures as a function of time are shown in Figure 4, while the temperature difference between the reference and sample as a function of the reference temperature is shown in Figure 5. As is evident from Figure 5, a well defined endothermic peak in the differential temperature trace begins at 1860 C ±29 C during the initial sample heatup. Thus, the measured melting temperature agrees with the reported value given the uncertainty in the temperature measurement. After melting, the discontinuous change in temperature is again observed. However, no additional DTA peaks are observed on the subsequent heating and cooling cycles for this sample. The reason for this was determined during posttest examination of the crucible. These examinations indicated that the ZrC crucible had cracked during the run, and the melt material had run out of the crucible and filled the interstitial gap between the crucible and the graphite holder. Thus, the absence of any discernible DTA peaks in the later phases of the experiment is due to the fact that no melt was present in the crucible. Given the fact that the Zr had come into contact with the graphite fixture, the sharp exothermic peak in the DTA trace after the sample had melted could also be attributable to zirconium reaction with the graphite outer fixture to form ZrC, which is an exothermic reaction.

The third test (Test No. 2) was conducted with a 50% oxidized corium composition. As shown in Table 5, the powder mass corresponded to 17.369 g. The thermal cycle for this sample consisted of a 25 C/minute heatup to 2700 C followed by a five minute hold at this temperature. The sample was then cooled to 1700 C at a rate of 10 C/minute. After 1700 C was reached, the sample was reheated to 2700 C at a rate of 10 C/minute. After 2700 C was reached the second time, the power was turned off to terminate the test. The sample and reference temperatures as a function of

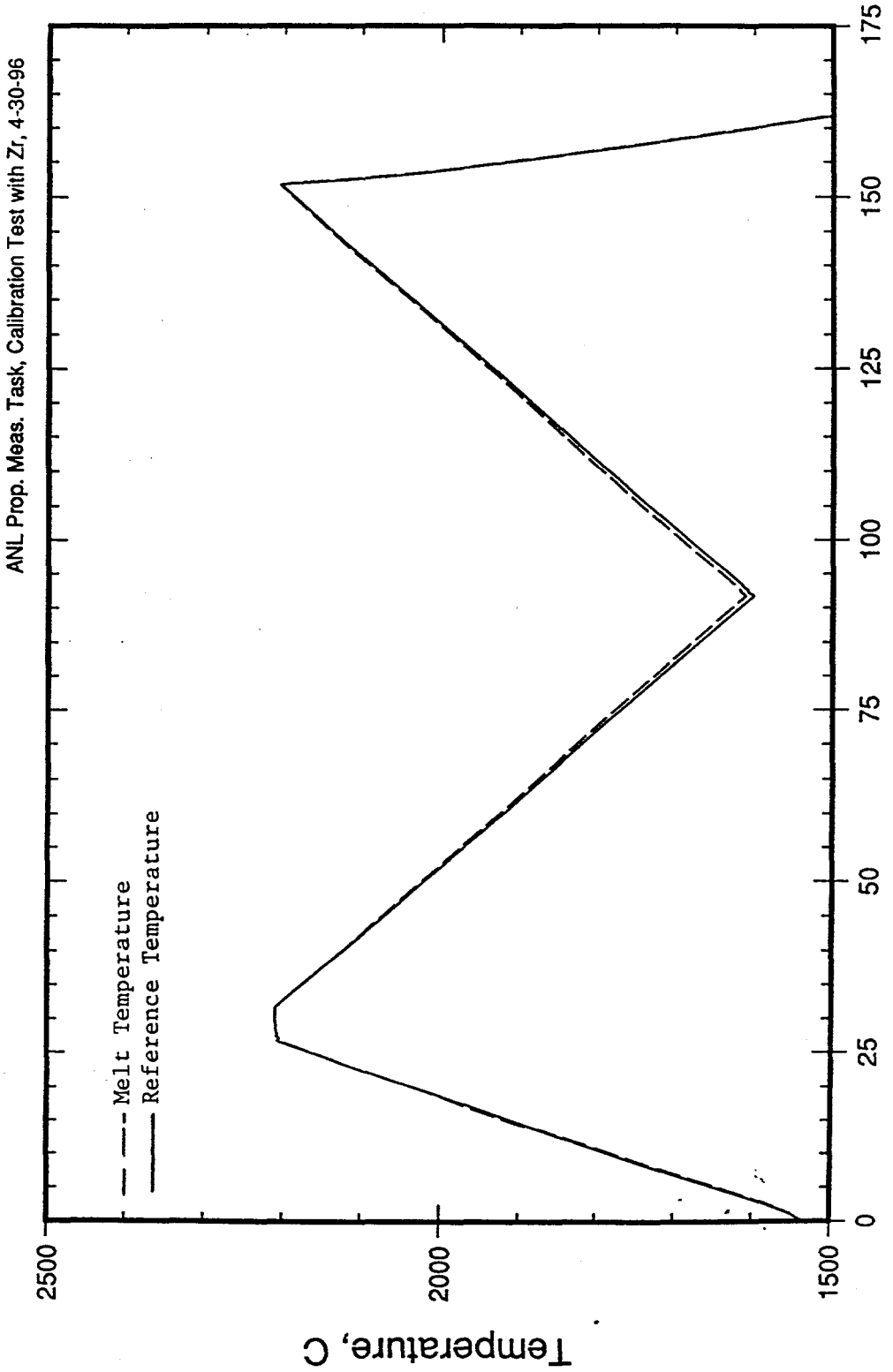

Figure 4. Melt and Reference Crucible Temperatures for Test 1-C (100% Zr)

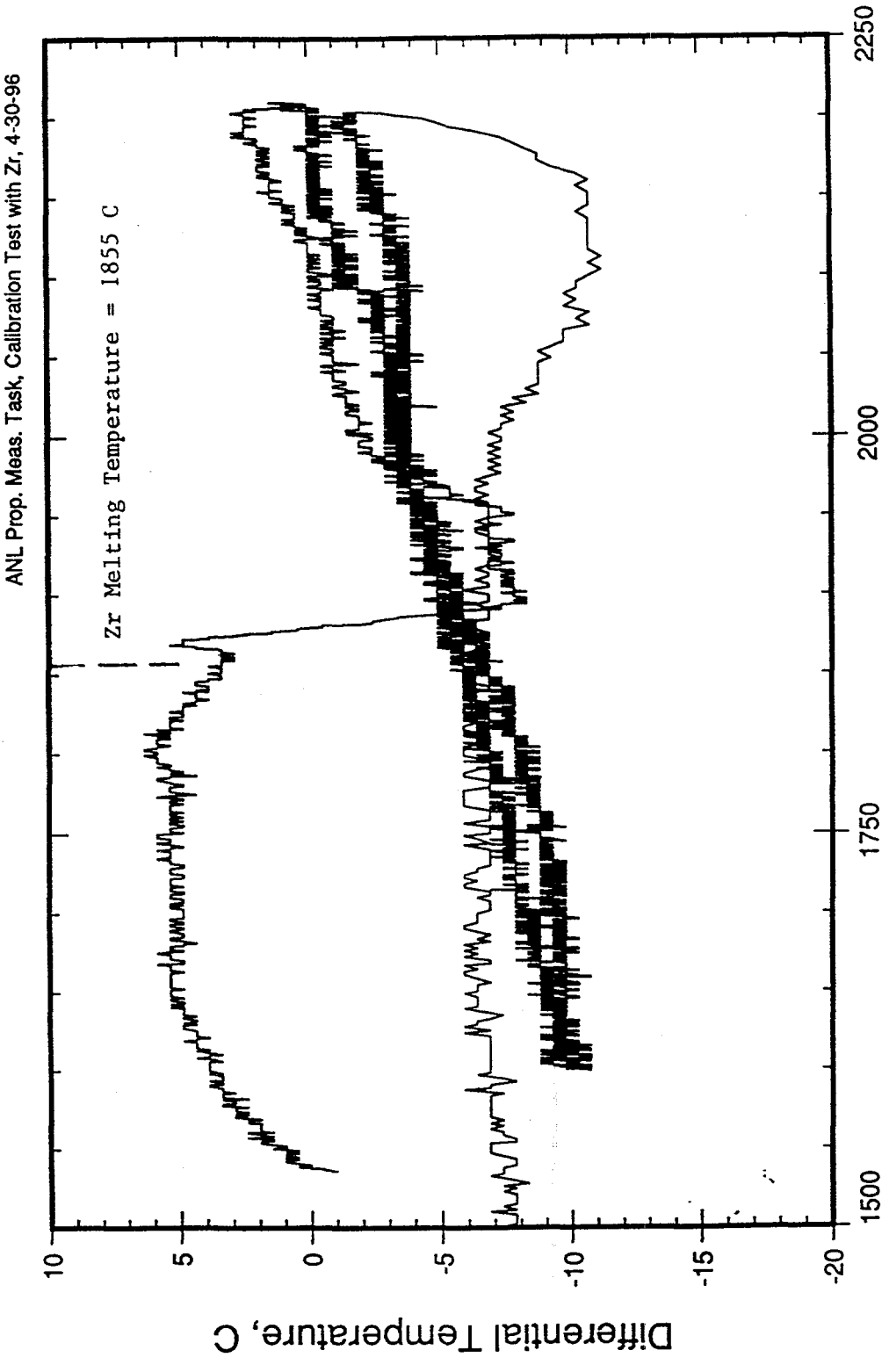

Figure 5. Temperature Difference Between Reference Crucible and Melt for Test 1-C (100% Zr)

time are shown in Figure 6, while the temperature difference between the reference and sample as a function of the reference temperature is shown in Figure 7. As is evident from Figure 7, the first endothermic break in the differential temperature curve occurs at 2000 C during the heatup, indicating onset of melting in the sample. Similar inflection points are observed at the same temperature upon subsequent heating and cooling cycles. However, the magnitude of these inflections are less in comparison to the initial break, which may in part be attributable to the difference in the heating/cooling rates.[1] The second break in the differential temperature trace begins at ~2450 C and terminates abruptly at ~2500 C; this change is attributable to the material color change upon complete melting. Thus, the liquidus for this composition is determined to be 2500 C ±35 C based on this inflection point. As is evident from Figure 7, a large endothermic peak beginning at 2500 C is also noted upon cooling of the sample at 10 C/min. However, the peak is absent upon reheating at 10 C/min., and upon cooling after the power supply was turned off. The absence may be attributable to chemical interaction between the crucible and the melt in the later stages of this test. Chemical analysis and metallographic results are discussed later in this section.

The fourth test (Test No. 3) was conducted with a 30% oxidized corium composition. As shown in Table 5, the powder mass corresponded to 17.60 g. The thermal cycle for this test was identical to the previous test (Test No. 2) described above. The sample and reference temperatures as a function of time are shown in Figure 8, while the temperature difference between the reference and sample as a function of the reference temperature is shown in Figure 9. As is evident from Figure 9, the first endothermic break in the differential temperature curve occurs at 1950 ±30 C during the heatup, indicating onset of melting in the sample. The second break in the differential temperature trace begins at ~2250 C and terminates abruptly at ~2280 C; this change is attributable to the material color change upon complete melting. Thus, the liquidus for this composition is estimated to be 2280 ±33 C based on this inflection point. However, note that significant repeatable inflection points in the differential temperature trace are not noted on subsequent heating/cooling cycles for this sample. The reason for this was determined during posttest examination of the crucible. These examinations indicated that the ZrC crucible had cracked during the run, and the melt material had run out of the crucible and filled the interstitial gap between the crucible and the graphite holder. Thus, the absence of any discernible DTA peaks in the later phases of the experiment is due to the fact that no melt was present in the crucible.

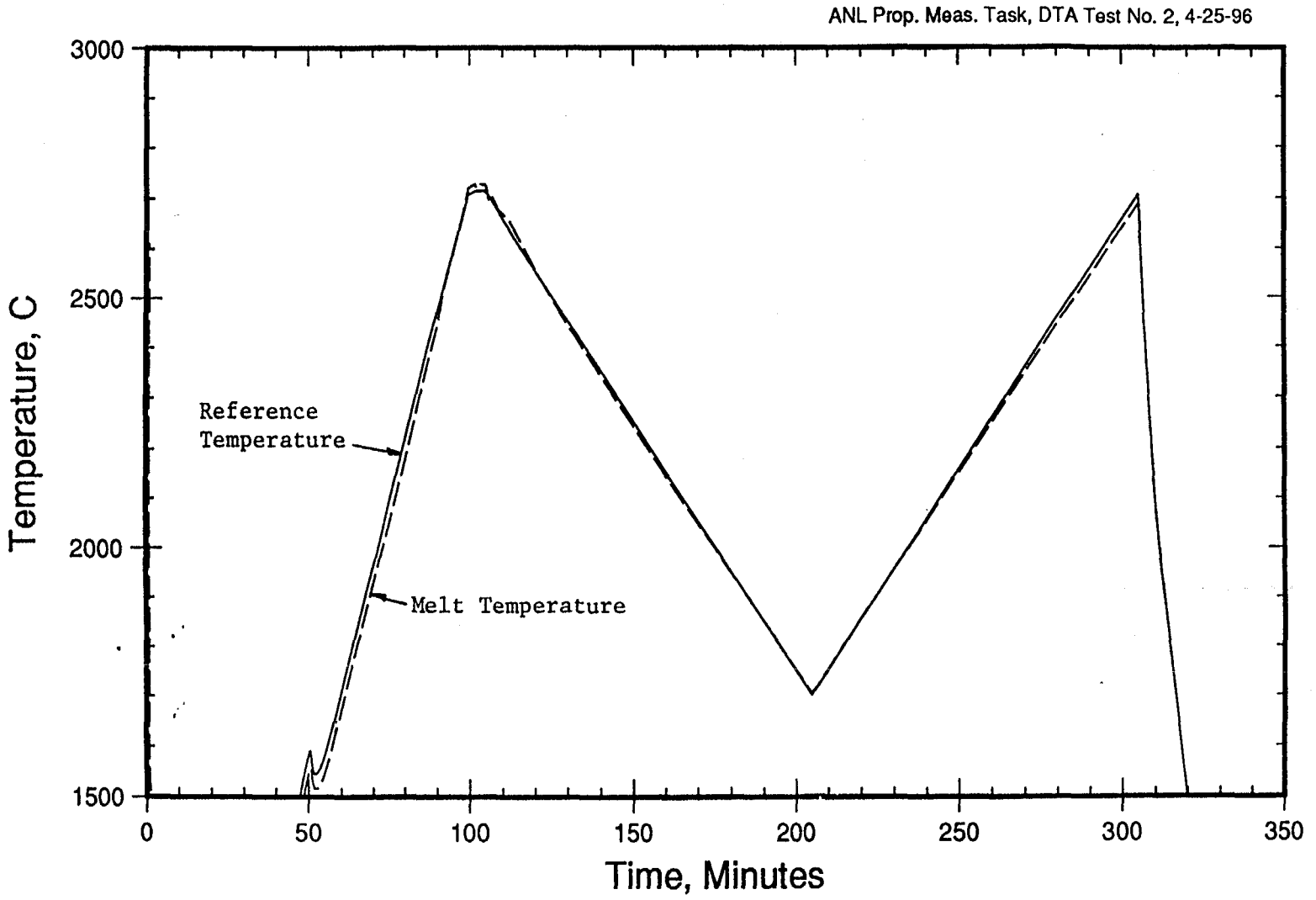

Figure 6. Melt and Reference Crucible Temperatures for Test No. 2 (50% Oxidized Corium)

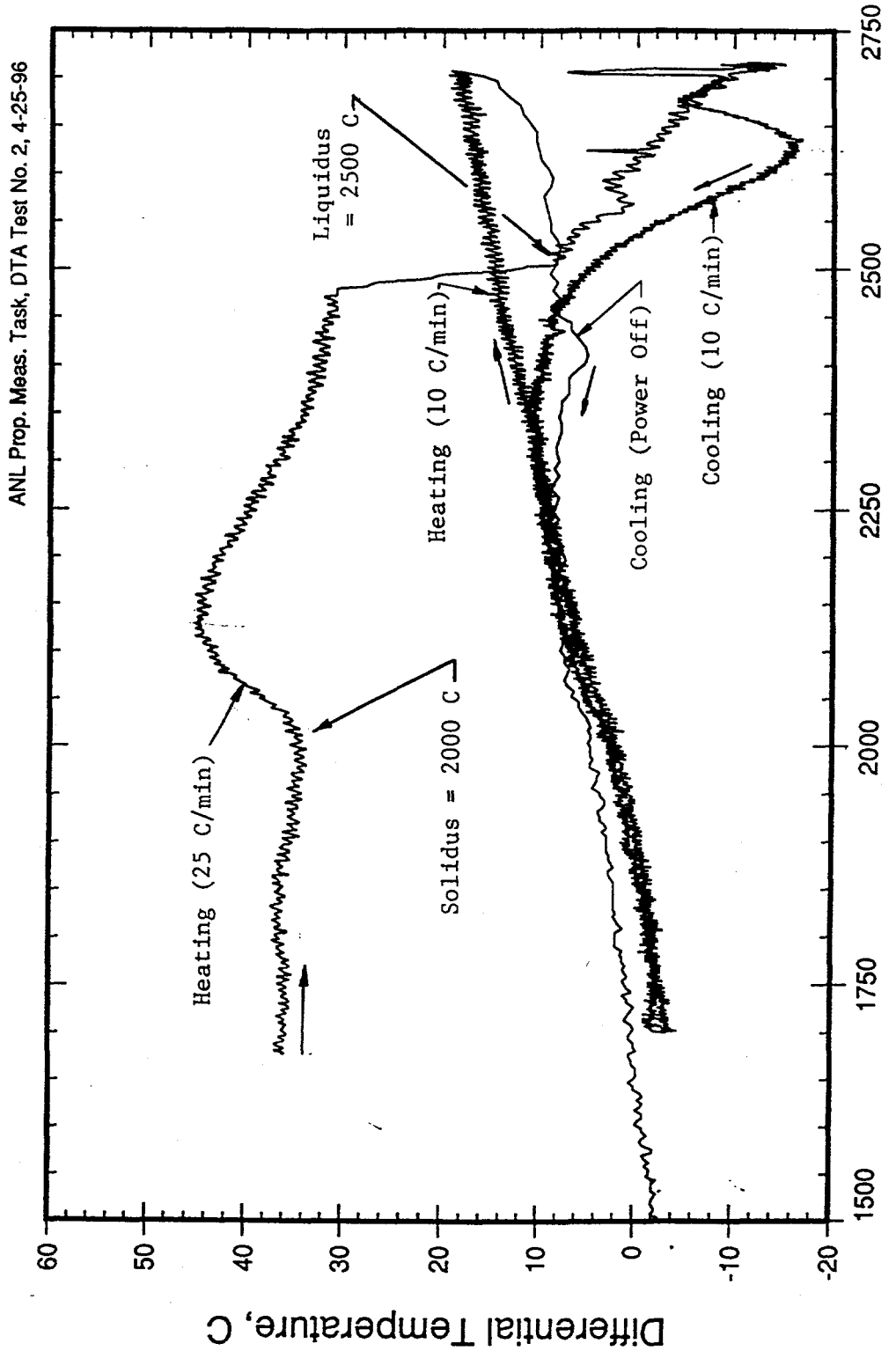

Figure 7. Temperature Difference Between Reference Crucible and Melt for Test No. 2 (50% Oxidized Corium)

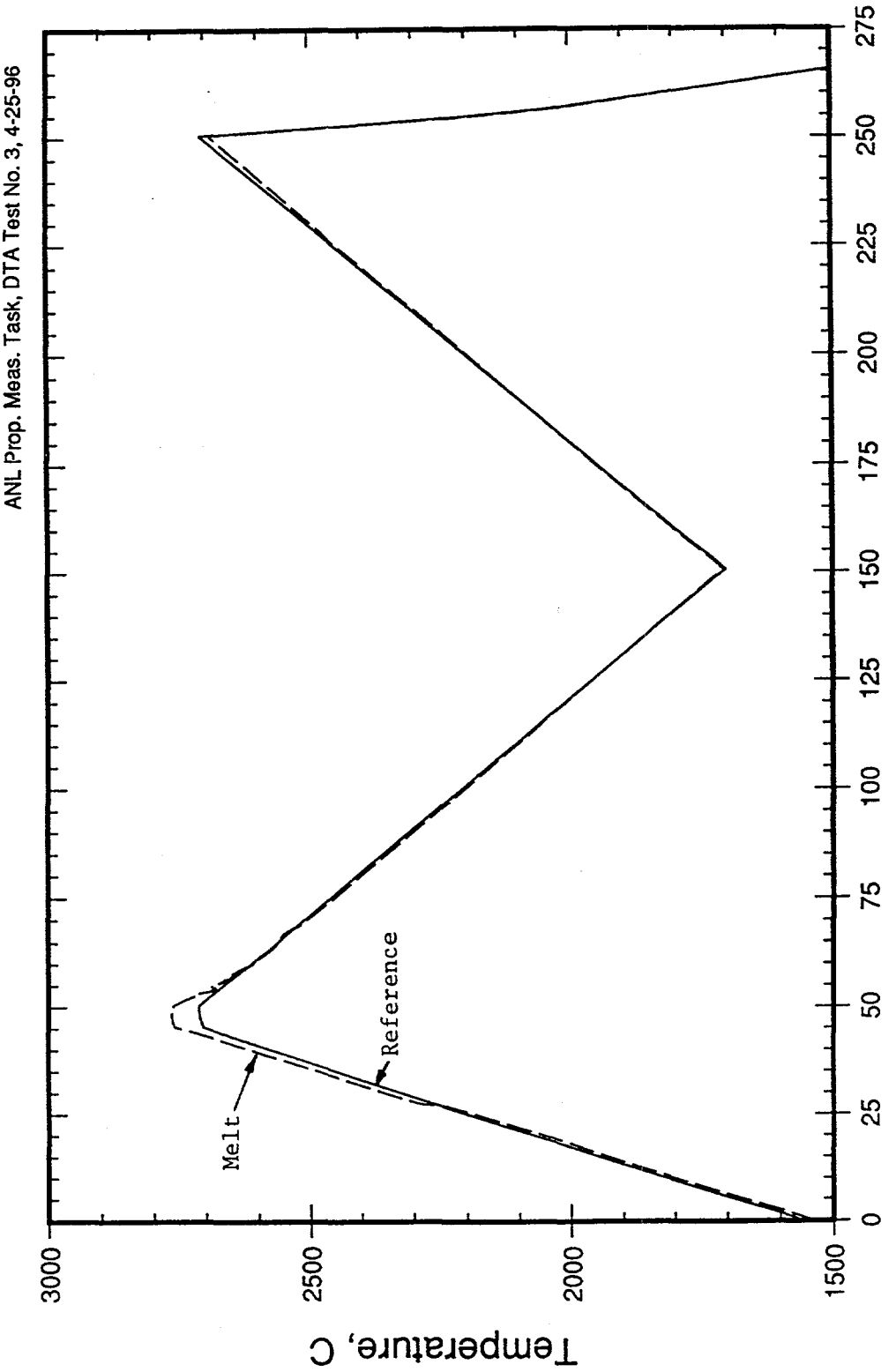

Figure 8. Melt and Reference Crucible Temperatures for Test No. 3 (30% Oxidized Corium)

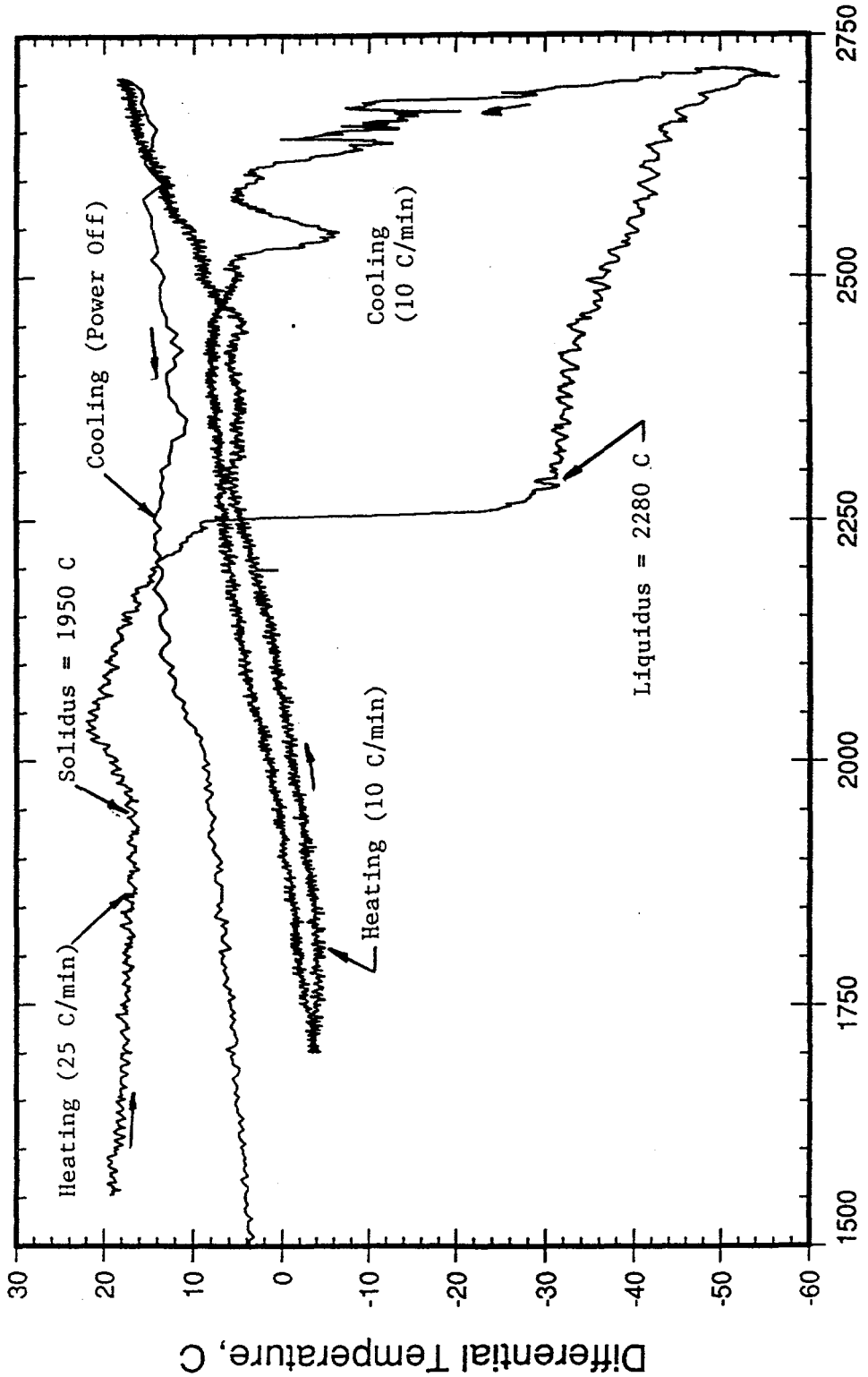

Figure 9. Temperature Difference Between Reference Crucible and Melt for Test No. 3 (30% Oxidized Corium)

Note that the measured solidus temperature of 1950 ±30 C for Test No. 3 is in reasonable agreement with the experimentally determined value of 1920 C measured by Skokan[4] (see Figure 2 therein) for a mixture of oxygen-saturated α-Zr and UO_2 in the range of 0-30 mole % UO_2. The 30% Zr oxidation state in Test No. 3 corresponds to 37.5 atom % O in the binary Zr-O system, which may be compared with 30 atom % O for a-Zr (22% equivalent Zr oxidation). Note that Test No. 3 was conducted with 40.8 mole % UO_2, which lies outside the range of experiment data obtained by Skokan. However, the postulated phase diagram for the quasibinary system α-Zr(O)-UO_2 produced by Skokan indicates that the solidus temperature is constant at ~1900 C for UO_2 contents up to ~82 mole %. The current data indicates that this trend is true to at least 40.8 mole % UO_2, keeping in mind the slight difference in O content for the binary Zr-O system between the two tests. Skokan did not experimentally determine liquidus temperatures as a part of his study.

Figure 10 compares the solidus/liquidus temperatures measured in this study with the projected phase diagram provided by the Kurchatov Institute.[3] As is evident from the figure, the solidus data point at 30% Zr oxidation lies within 50 C of the prediction, while the solidus point at 50% oxidation states lie ~100 C above the prediction. The solidus point at 70% oxidation is in agreement with the prediction. In terms of liquidus temperatures, the two data points at 50 and 70% oxidation lie within 40 C of the prediction. At 30% oxidation, the liquidus measured in the experiment is ~150 C below the prediction. Note, however, that the crucible cracked for the 30% oxidized test, so that the initially recorded 2280 C liquidus temperature could not be confirmed on subsequently heating/cooling cycles.

Once the original series of tests was completed, both chemical analysis and metallography activities were initiated to identify any impurities introduced over the course of the experiments, and to identify the phase structure of the solidified debris. After sectioning of the crucibles, samples of the solidified melt were taken from Test Nos. 1 and 2 and submitted for analysis by the Analytical Chemistry Laboratory at Argonne. A sample could not be obtained for Test No. 3 due to the fact that the crucible cracked during the test leading to melt leakage from the crucible. The two samples were analyzed using Inductively Coupled Plasma Atomic Emission Spectroscopy (ICP/AES). This method identifies the elemental composition of the samples, with the exception of carbon and oxygen. Carbon level was determined separately with a LECO Carbon Analyzer. Oxygen level was also determined separately by measuring the mass gain on ignition at 900 C in an air atmosphere.

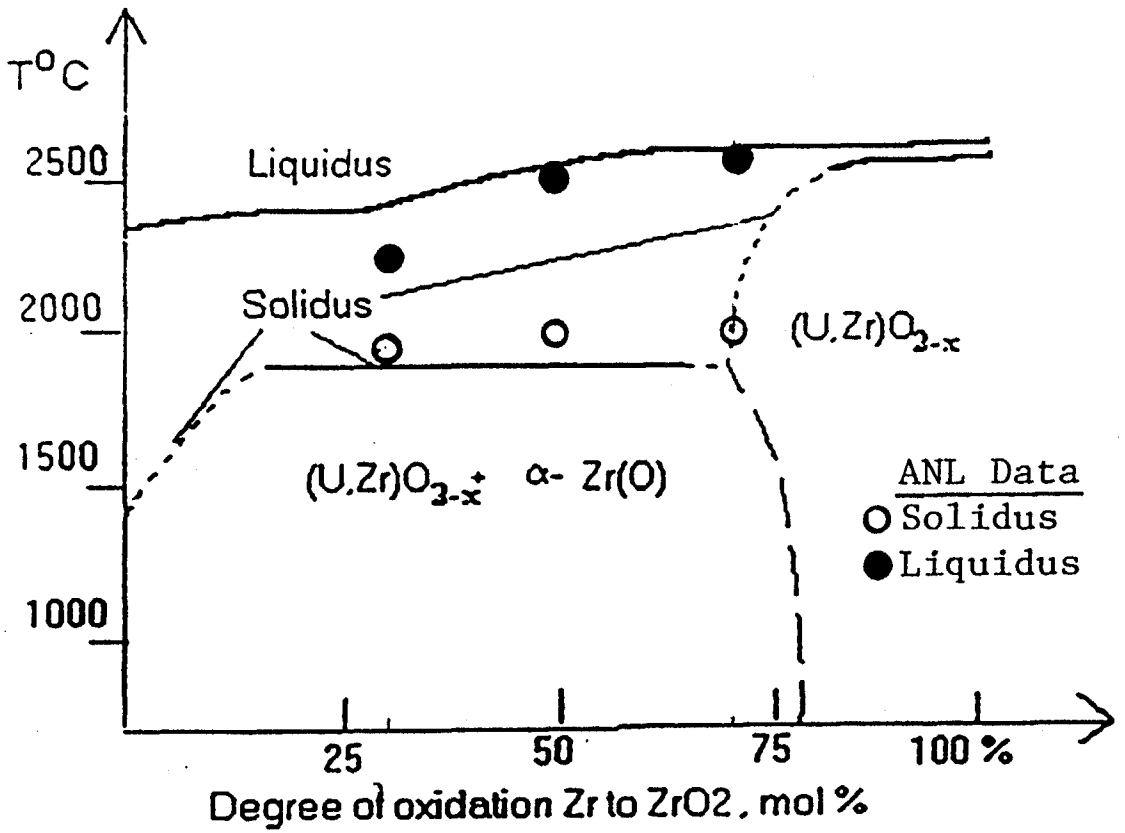

Figure 10. Comparison of Measured Liquidus/Solidus Temperature with the Phase Diagram Provided by the Kurchatov Institute

Samples from Test Nos. 1 and 2 were also mounted for microscopic examination. The samples were vacuum potted in Buehler Epo-Kwick Epoxy. The samples were then successively ground with 120 through 600 Grit sand paper, finishing with 6 μm diamond and 0.05 μm Al_2O_3 polishes. The samples were then rinsed with water and ethanol before viewing under a microscope.

The chemical analysis results for Test No. 1 are shown in Table 6. As is evident from the table, the results indicate that the sample contained 8.3 wt % carbon. As shown in Table 5, carbon was not present as an initial powder constituent for this or any of the tests. Visual examination of the sectioned crucibles indicated that dissolution of the crucibles had occurred during the tests. Based on the assumption that carbon present in the sample came from dissolution of the crucible, the corresponding melt composition is shown in Table 7 after subtracting out the carbon present, plus an additional mole of zirconium for each mole of carbon, consistent with the chemical form of the crucibles. Note that the trace impurities shown in Table 6 have been neglected in this assessment. Also shown in Table 7 is the expected melt composition given the initial powder constituency shown in Table 5. As is evident from Table 7, the melt composition after removal of the crucible constituents is in reasonable agreement with the expected composition, albeit the U content is slightly higher than expected, and the Zr content is slightly lower than expected. Thus, this analysis indicates that substantial dissolution of the ZrC crucible occurred during the course of this experiment, and that the primary source of carbon contamination in the melt was from the crucible (as opposed to the furnace heaters).

The chemical analysis results for Test No. 2 are shown in Table 8. This data indicates a carbon content of 8.13 wt % in the solidified debris, in virtual agreement with the previously described results for Test No. 1. As was done for Test No. 1, Table 9 presents the corresponding melt composition for Test No. 2 assuming that carbon present in the sample arose from dissolution of the crucible. As is evident from this table, the melt composition after removal of the crucible constituents is in reasonable agreement with the expected composition, albeit the U content is slightly lower than expected, and the Zr content is higher than expected. Thus, the analysis for this test also indicates that substantial dissolution of the ZrC crucible occurred during the course of this experiment, and that the primary source of carbon contamination in the melt was from the crucible.

In terms of assessing the effect of crucible dissolution on the test results, a developmental test was conducted using 70% oxidized corium (i.e., composition identical to that used in Test No. 1)

Table 6. ICP/AES Results for Test No. 1

Constituent	wt %	Error (±%)
U	18.7	5
Zr	68.3	5
O	4.23	30
C	8.30	5
Al	0.146	20
Ca	0.0034	"
Cr	<0.002	"
Cu	0.0066	"
Fe	0.017	"
Mg	0.0011	"
Na	0.024	"
Ti	0.361	"
W	<0.01	"
Zn	0.0023	"

Table 7. Comparison of Expected and Actual Melt Compositions for Test No. 1 Assuming Carbon Present in Sample is Due to Crucible Dissolution

Element	Mole % in Sample	Mole % in Sample After ZrC Removal	Expected Mole %
U	4.40 ± 0.2	19.55 ± 1.0	15.45
Zr	42.04 ± 2.1	14.66 ± 1.0	22.35
C	38.74 ± 1.9	-----	-----
O	14.81 ± 4.4	65.79 ± 19.7	62.20

Table 8. ICP/AES Results for Test No. 2

Constituent	wt %	Error (±%)
U	13.6	5
Zr	74.6	5
O	2.83	49
C	8.13	5
Al	0.162	20
Ca	0.0022	"
Cr	<0.002	"
Cu	0.0064	"
Fe	0.0070	"
Mg	0.009	"
Na	0.017	"
Ti	0.022	"
W	<0.01	"
Zr	0.021	"

Table 9. Comparison of Expected and Actual Melt Compositions for Test No. 2 Assuming Carbon Present in the Sample is Due to Crucible Dissolution

Element	Mole % in Sample	Mole % in Sample After ZrC Removal	Expected Mole %
U	3.30 ± 0.2	15.19 ± 0.8	16.97
Zr	47.35 ± 2.4	37.83 ± 2.6	24.60
C	39.13 ± 2.0	-----	-----
O	10.21 ± 5.0	46.99 ± 23.0	58.42

prior to initiating the test series described herein. In this test, the sample was heated to 2350 C at 10 C/minute before the furnace was turned off. As the results discussed previously indicate, the solidus and liquidus temperatures for this composition are approximately 2000 C/2600 C, respectively. Thus, the sample is estimated to have been heated to a temperature which is ~60% through the melting temperature range. Posttest examinations indicated that the material had indeed been heated above the solidus but had not yet reached a fully molten state (i.e., the powder had densified and sintered into a semi-porous but rigid pellet). During this test, no interaction between the sintered material and the crucible was noted. On this basis, crucible dissolution is felt to occur predominately near or above the liquidus temperature. In the fully molten state, convective patterns can develop in the melt which enhance the rate of chemical interaction. As a result, the measurements of solidus/liquidus recorded during initial sample heatup for these tests are considered to be reliable. After the liquidus is reached, the measured melting temperatures are probably representative of a corium melt containing a significant fraction of Zr and C from the crucible in solution with the melt. If the ZrC which is introduced into the mixture after melting occurs is retained as a separate solid solution, then solidus/liquidus temperatures measured on subsequent heating cooling cycles may still be valid. However, a detailed assessment of the chemical behavior under these circumstances is beyond the current scope of work.

The microstructure of the debris from Test No. 1 is shown in Figure 11. Photo (a) illustrates the phase structure of the debris from within the crucible. As is evident from this figure, three distinct phases are present. The sample was scanned axially from the melt/crucible interface to the top of the solidified debris. This scan consistently indicated the phase structure shown in photo (a). At the time this report was completed, SEM analysis to identify the elemental composition of the three separate phases had not been completed. However, the axial consistency of the phase structure indicates that global segregation into distinct metal and oxide phases did not occur during cooldown. Global segregation would be expected due to density differences between molten Zr and the oxide phase if any of the Zr present as an initial condition was not soluble in the oxide phase. On this basis, it is concluded that at 70% Zr oxidation, the Zr metal is soluble in the oxide phase under molten conditions. The effect that the dissolved ZrC has on this conclusion has not been assessed. Photo (b) in Figure 11 illustrates the phase structure of the crucible following the test, while photo (c) shows the lower interface between the graphite fixture and the crucible. The axial variation of

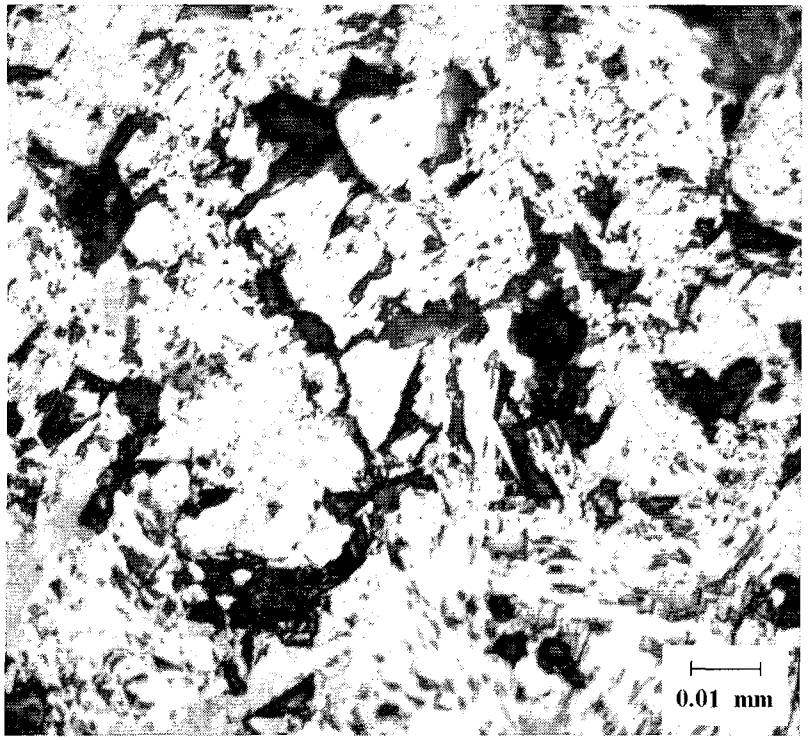

(a)

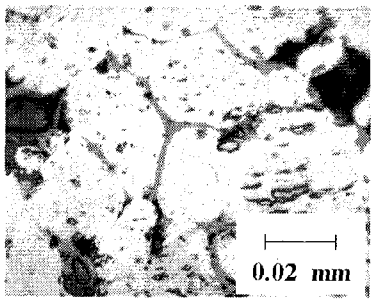

(b)

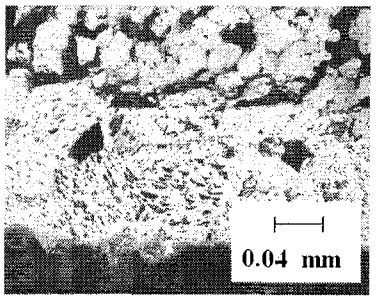

(c)

Figure 11. Debris Microstructure for Test No. 1 (60 X Magnification); (a) Debris within Crucible, (b) Crucible, and (c) Lower Interface between Graphite Fixture and the Crucible

materials in photo (c) is as follows: i) graphite fixture is evident as a black band at the bottom of the photo, ii) solidified melt layer occupies the center portion of the photo, and iii) crucible material is evident at the top of the photo. The phase structure of the debris beneath the crucible is noted to be similar to that found within the crucible (photo (a)).

The microstructure of the debris from Test No. 2 is shown in Figure 12. Photo (a) illustrates the phase structure of the debris adjacent to the crucible boundary, while photo b) illustrates the structure of the crucible itself. The axial scan of the debris for this test indicated consistently the same phase structure as that shown on the left hand side of photo (a). Thus, the same conclusion is drawn regarding the solubility of Zr metal in the oxide phase for this test as was drawn for the previously described experiment. However, as shown in photos (a) and (b), melt interaction with the crucible was more pronounced for this test; the presence of corium within the crucible boundary is clearly evident as a greyish phase in both of these photos.

2.3 Recommendations for Additional Testing

The initial series of tests conducted with the facility indicate that the experiment approach for measuring liquidus/solidus temperatures for corium compositions over a wide range of Zr oxidation states is viable. In order to improve the quality of the data in subsequent testing, the following recommendations are made:

i) Examine alternative crucible materials. These initial tests indicate that ZrC undergoes dissolution at high temperatures with the corium compositions examined in this study, particularly for low Zr oxidation states (i.e., high Zr metal fractions). This complicates interpretation of the data since the crucible material acts as an impurity in the melt which is introduced over the course of the test. In addition to dissolution, the crucibles were observed to crack for several tests, leading to melt leakage from the crucibles. This limited the fidelity of the data on the heating/cooling cycles late in these tests, since DTA peaks could not be observed after the melt leaked from the crucibles. Skokan[4] utilized tungsten, zirconia, and thoria crucibles in his studies of phase transitions in mixtures of α-Zr and UO_2 for low molar fractions of UO_2. Problems with crucible compatibility with the melts were not described in this paper.

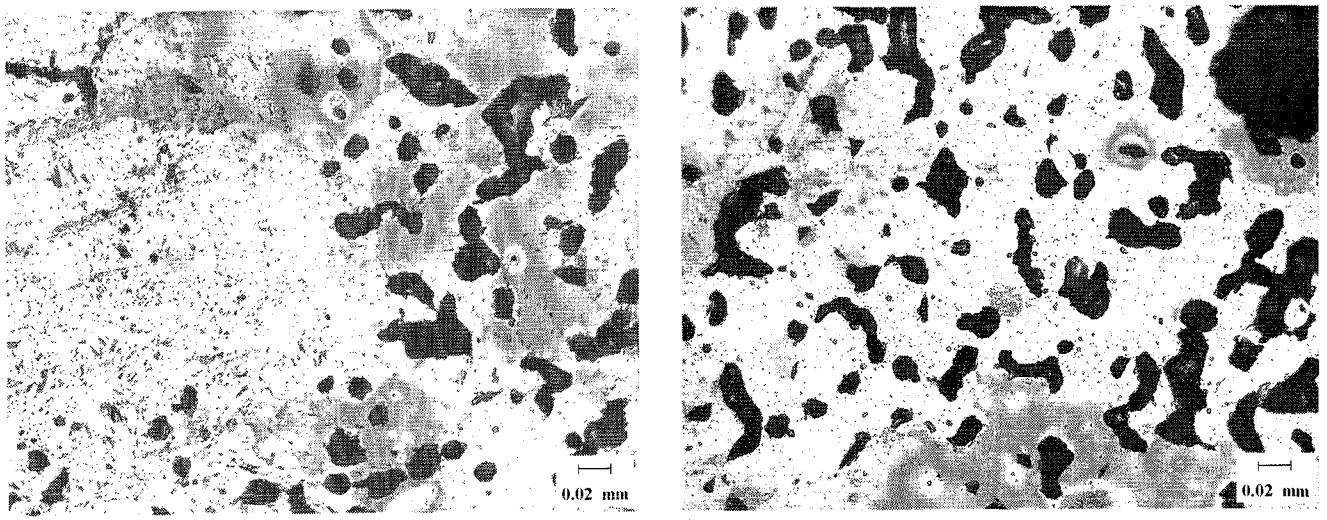

(a) (b)

Figure 12. Axial Variation of Debris of Microstructure for Test No. 2 (60 X Magnification); (a) Debris Adjacent to Crucible Boundary and (b) Crucible

ii) Video capability should be added to the pyrometer focused on the melt surface. This will provide direct visual confirmation that the sample liquidus has been reached, since melting of the sample will be visually recorded.

Aside from the above recommendations to improve the experiment technique, it is important to expand the parameter ranges investigated in this study in order to provide sufficient data for development of a general phase diagram database for in-vessel accident sequences. The mass fraction of UO_2/ZrO_2 investigated in this study corresponds to 1.51, which is consistent with the VVER-440 core composition as well as many US BWRs (i.e., Grand Gulf BWR/6 is 1.55). However, for many US PWRs, this ratio is as high as 3.6 (i.e., Zion PWR). Thus, to develop a general database for broad use the UO_2/ZrO_2 ratio should be expanded in follow-on testing to encompass a range of UO_2/ZrO_2 ratios in the range of 1.5 - 4.0 with various Zr oxidation states tested for each ratio.

3.0 VISCOSITY CHARACTERIZATION

3.1 Facility Description

A schematic illustration of the experiment setup for the viscosity characterization tests is shown in Figure 13. The facility consists of a 1-D spreading channel which has internal dimensions of 3.58 m long by 15.9 cm wide. The melt was generated through the use of exothermic chemical reactions at one end of the spreading channel; details of the melt generator region are provided in Figure 14. The powders were initially separated from the open channel by a meltout barrier (i.e., stainless steel shim stock). This barrier failed by melt through at the end of the burn, thus initiating a 1-D "dam break" spreading experiment. This approach for initiating the test is desirable from two viewpoints: (i) it is simple and reliable (i.e., a separate melt generator is not required), and (ii) test results can readily be analyzed to determine flow regimes and corium viscosity since the test initial conditions are consistent with those assumed by Huppert[2] in his analysis of viscous free surface flows.

One of the key experimental objectives was to realize isothermal spreading conditions to the greatest extent possible. Isothermal spreading conditions are required to reduce uncertainties in the experiment data since corium viscosity is a strong function of temperature[6]. The principal structural material for the test section was castable MgO obtained from National Refractories., Inc. Following placement of the MgO, the substrate surface and sidewalls were lined with a 1.3 cm thick layer of castable ZrO_2. This material has a low thermal conductivity of 1.2 W/m·K at 1200 C. After placement of the ZrO_2, the channel width was equal to 15.88 cm. The top cover of the apparatus consisted of a layer of 20 mil tungsten shim stock backed up by a 1.3 cm thick layer of low density ZrO_2 insulator board (thermal conductivity of 0.3 W/m·K at 1700 C). Thus, the upper cover of the apparatus was insulated to the greatest extent possible in order to minimize upwards heat losses during the spreading phase.

In terms of estimating corium viscosity, the principal experiment data to be obtained from the tests is the melt leading edge location versus time. This was obtained through the use of an array of burn wires positioned at the center of the channel flush with the spreading surface. The burn wires were constructed from Formvar (lacquer insulated copper) wire. Two pieces of this wire were twisted together to form a junction which was initially open. When the junction was contacted by

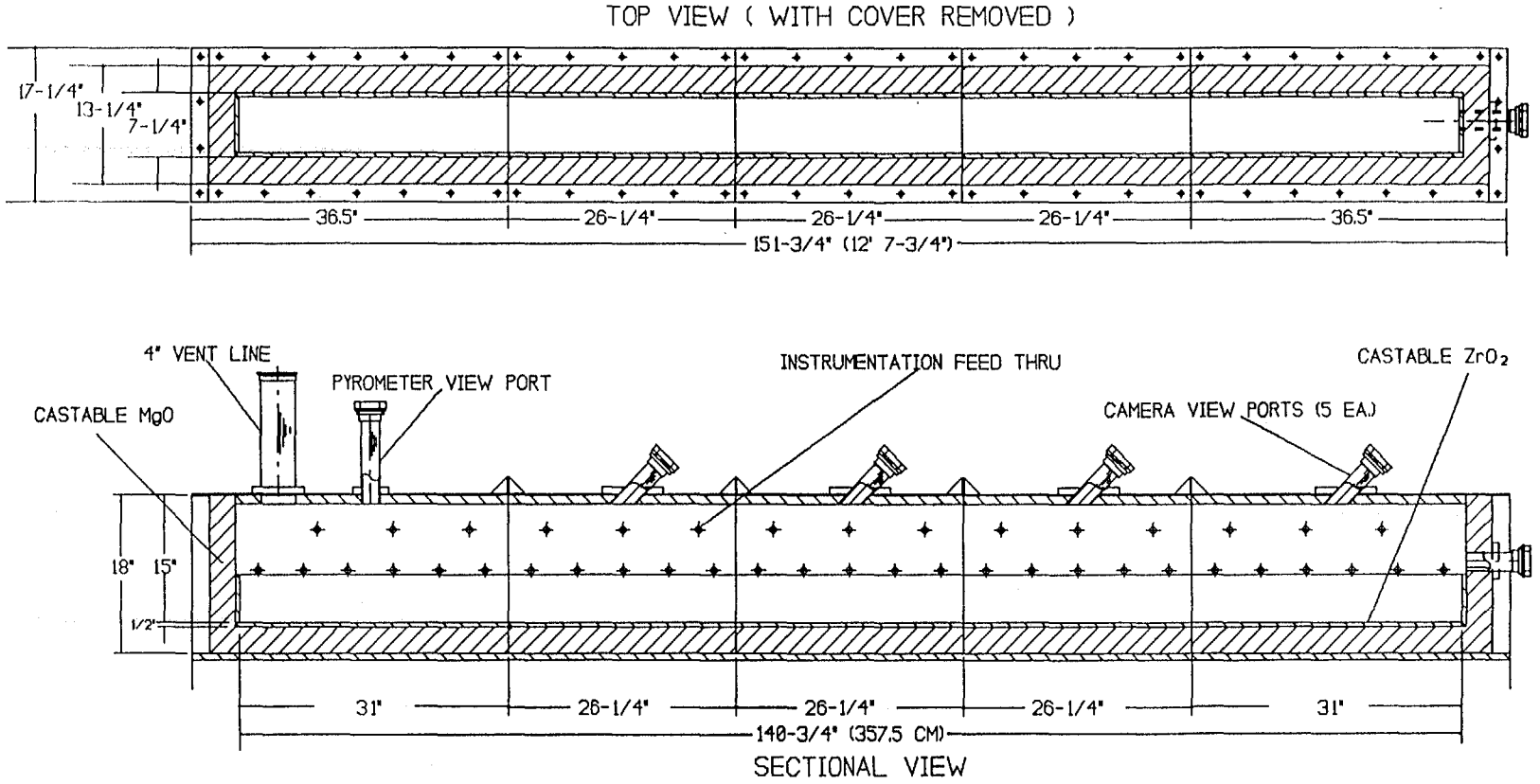

Figure 13. Schematic Illustration of Viscosity Determination Spreading Test Section

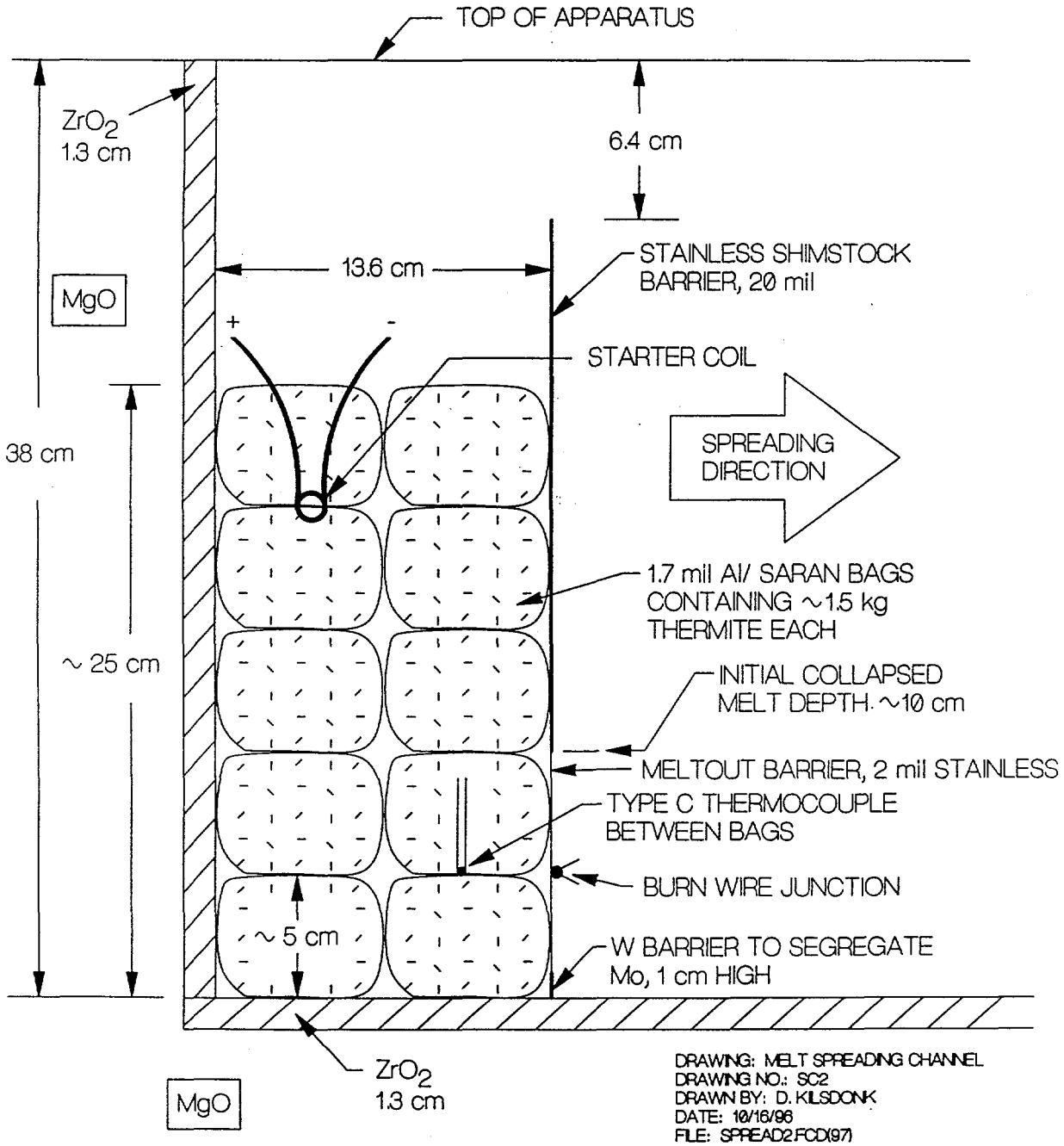

Figure 14. Illustration of Melt Generator Region

melt, the lacquer insulation was burned off, thereby completing the electrical connection. Each burn wire was attached to a common 5 Volt power supply across a 2:1 voltage divider. The voltage drop across this circuit was recorded, thereby providing a direct indication of when the melt front arrived at a given location. Melt temperatures were measured at several locations along the length of channel using 1.6 mm diameter Tantalum sheathed, MgO insulated, Type C (W5%Re/W26%Re) thermocouples located 6 mm above the spreading surface. This data was used to determine the temperature loss as the corium spread. The initial melt temperature was also measured using a Type C thermocouple, as well as an Ircon two-color pyrometer (1500-3500 C temperature range); the pyrometer viewport location is shown in Figure 13. The spreading behavior was recorded by a total of five video cameras mounted at various positions along the spreading channel; the viewport locations are shown in Figure 13. During the test, a total of 200 slpm Argon was purged through the video camera and pyrometer viewports to prevent aerosol deposition on the viewport windows. The purge gas, as well as any gases/aerosols generated during the experiment, exited the test section through a 10 cm diameter, water cooled, vent line located on the lid of the apparatus behind the melt generator region (see Figure 13). The vent line was routed to a scrubber/HEPA filter system for cleanup prior to discharge from the building. Note that the vent line exit was deliberately placed near the melt generator region in an effort to remove as much aerosol as possible from the test section to improve the video data.

As noted earlier, the corium compositions shown in Table 1 were generated through exothermic chemical reactions. Prior to initiating the spreading tests, both analysis and supporting developmental tests were performed in order to identify mixtures which generate prototypic melts with 30, 50, and 70% Zr oxidation. In these reactions, the U, Zr, and O contents were fixed at the target values shown in Table 1 for a given level of Zr oxidation. Initial powder constituents included UO_3, U, Zr, and MoO_3. The reaction heat was adjusted by varying the amount of U/UO_3 present in the initial powder mix; Zr was always incorporated in metallic form. Molybdenum Trioxide (MoO_3) was utilized as the principal oxygen provider in the reactions. The required MoO_3 content in the mixture was determined by the amount of oxygen required to obtain a particular level of Zr oxidation given the initial U/UO_3 content in the thermite. Mo metal was generated as a reaction byproduct in the thermite reactions. Advantages of Mo metal in this application include low vapor pressure, low solubility in the oxide phase, and rapid phase segregation due to the large density difference between

the metal and oxide phases. A segregation technique was used to separate the Mo from the $(U, Zr)O_{2-x}$ phase prior to initiating the spreading test; the method for accomplishing this is described below. A total of eight developmental tests were performed in order to obtain initial mixtures which reacted at nominally 2500 C. Aside from verifying the reaction temperature, the developmental tests confirmed that the Mo rapidly segregates during the reaction, and that the resultant oxide phase is molten and flows at the indicated temperature. The actual compositions used in the spreading tests are provided in the description of test results.

As summarized above, a segregation technique was used to remove the Mo metal from the reaction byproducts prior to initiating the spreading phase of the experiments. As shown in Figure 14, this was accomplished through the use of a tungsten barrier located at the lower front edge of the melt generator region. The cross-sectional area of the generator region was configured to produce a nominal 10 cm deep melt depth after the reaction was complete for all tests. The tungsten barrier was 1 cm high, which corresponds to the depth of molten Mo metal nominally produced during the reaction for the given generator region floor area. Thus, the Mo rapidly separated from the oxide phase and was retained by the tungsten barrier in the melt generator region after spreading was initiated. (Data on the degree to which this approach was successful is provided later). The powder mixtures were packed into the test section in 1.7 mil aluminized Saran bags. Aside from minimizing the spread of contamination, this approach prevented moisture infiltration into the powders as the experiment was set up (moisture leads to spurious gas release during the reaction). The reaction was initiated by a nichrome starter located at the top of the bed of powders (Figure 14). After ignition, the burn front proceeded downwards. After the burn was completed, the lower portion of the meltout barrier (i.e., < 10 cm) failed thereby initiating the spreading test. The lower portion of the barrier was constructed from 2 mil stainless shim stock. The upper portion of the barrier was constructed from heavier (20 mil) stock. The upper region was fabricated from heavier material so that it would remain intact during the reaction phase. In addition, the upper region was designed to have a relatively low heat capacity to minimize the crust mass deposited on this surface during the burn.

The general procedure for conducting the spreading tests was as follows. After setup was complete, the test section was inerted by a slow bleed (10 slpm) of argon overnight. When the test was to be initiated, the covergas flowrate was increased to 200 slpm. The data recording systems

were then started. The thermite was then ignited by apply 20 Amps AC current to the starter coil. After the test was completed and the debris had cooled to room temperature (overnight), the lid of the apparatus was removed. The debris was then photographed, and the debris spatial variation was measured. The debris was then removed from the test section. The Mo retained in the melt generator region was separated and placed in a separate container for weighing. The test data was downloaded from the data acquisition system at a frequency of 10 samples per second per channel. The data was then plotted and analyzed to determine the melt temperature variation and bulk viscosity based on the burn wire data, initial melt mass, and spreading channel width.

3.2 Test Results

A summary of initial/test conditions for the four spreading tests which were conducted is provided in Table 10. With the exception of Test RS-1, all experiments were conducted with an initial melt mass of 15.0 Kg. Taken together, Tests RS-0, RS-2, and RS-3 constitute a parametric study of the effect of Zr oxidation on the corium viscosity at a nominal melt temperature of ~2500 C. These tests did not contain stainless steel as an initial melt constituent. The melt spreading mass for these tests is less than the initial mass due to the fact that Mo metal was present as a reaction byproduct. The Mo segregated during the reaction and was retained in the melt generator region. Thus, the melt spreading mass shown in Table 10 for these tests is the actual prototypic corium mass which participated in the spreading transient. Test RS-1 was conducted with an initial stainless steel mass fraction of ~18 wt %. The Zr oxidation in this experiment (36.5%) is close to the Zr oxidation for test RS-2 (30%). Thus, comparison of the spreading data from these two tests provides data on the effect of molten Stainless steel on the corium viscosity.

The first test conducted in the experiment series, RS-0, utilized 50% oxidized corium. The pre- and post-reaction compositions for this test are shown in Table 11. The voltage signals from the burn wires are shown in Figure 15. The location of the melt leading edge after initiation of spreading, as deduced from the burn wire data in conjunction with the Type C melt temperature thermocouple data, is shown in Figure 16. Note that the melt arrival times shown in Figure 16 have been shifted by 107.3 seconds, which corresponds to the onset of spreading as indicated by the data from the burn wire located at the dam surface (see Figure 14 and 15). The test data, in conjunction with posttest examination of the debris, indicated that the dam configuration had worked properly insofar as initiating the experiment. The upper portion of the structure was intact (see Figure 14),

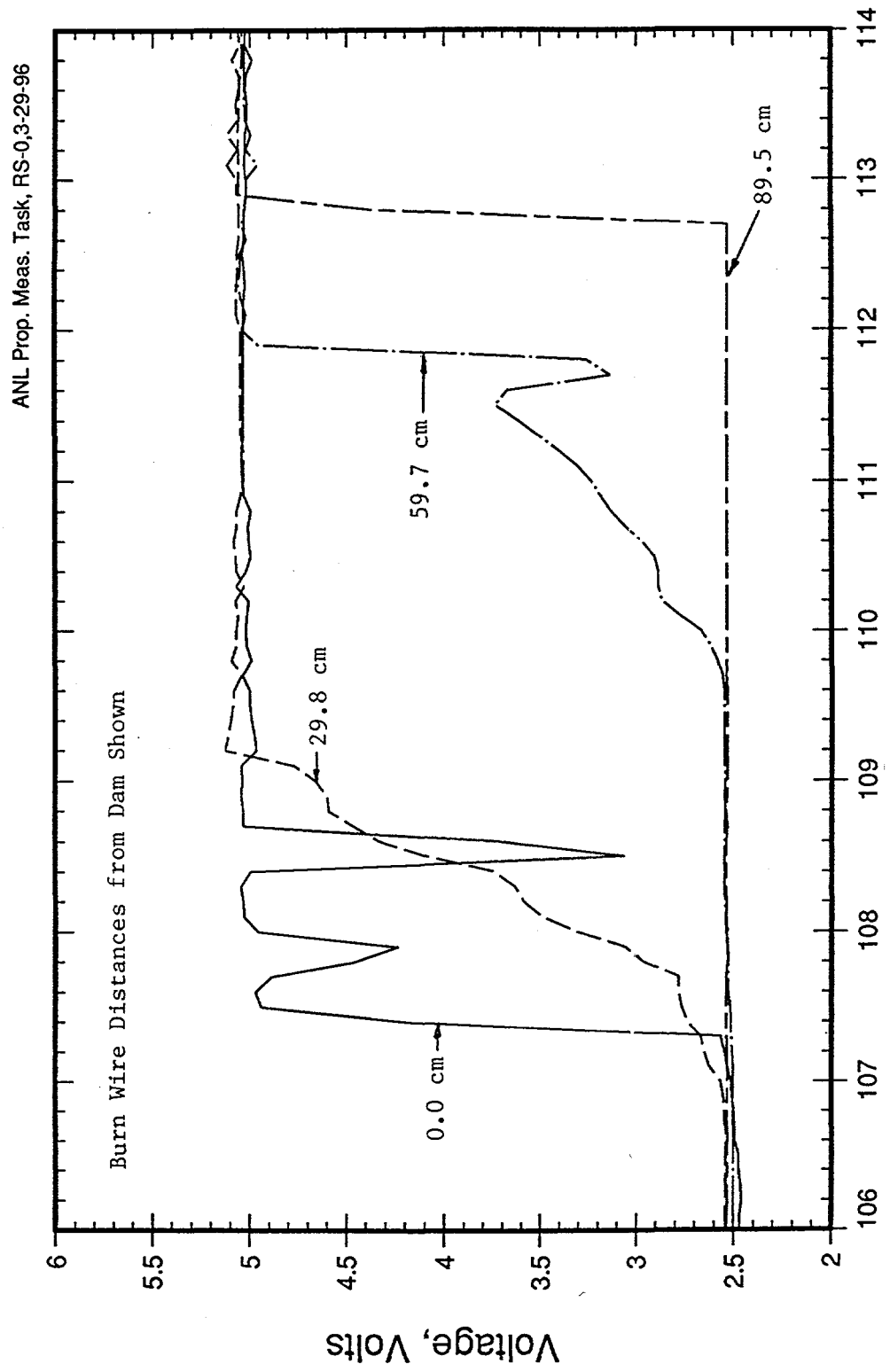

Figure 15. RS-0 Burn Wire Data

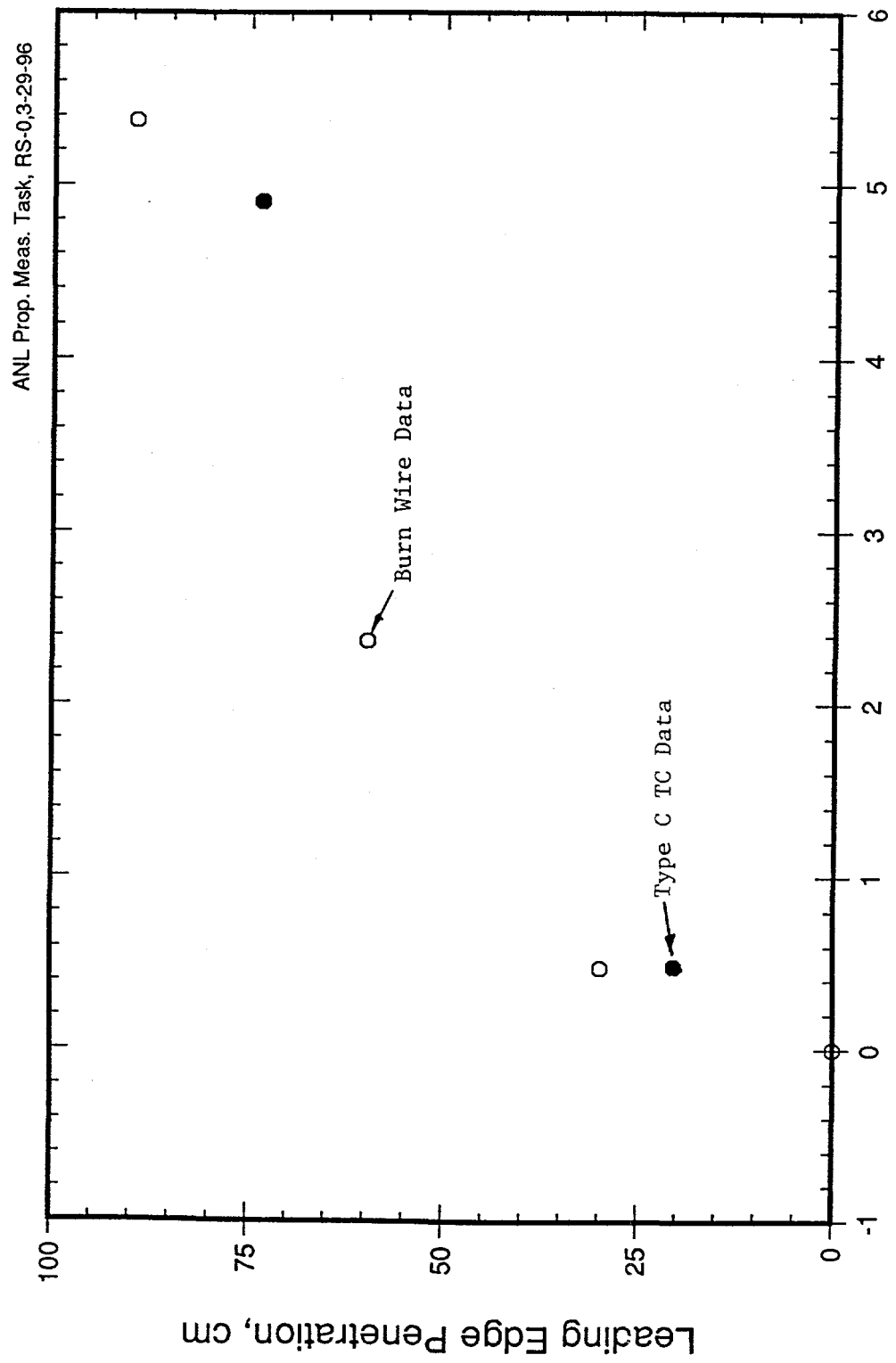

Figure 16. RS-0 Melt Leading Edge Location Versus Time

Table 10. Summary of Spreading Test Initial Conditions

Test Designation	Zr Oxidation (%)	Spread Melt Composition (wt%)	Initial Melt Mass (Kg)	Spread Melt Mass (Kg)	Initial Melt Temperature (K)
RS-O	50	63.5 UO_2, 21.0 ZrO_2, 15.5 Zr	15.0	12.47	2470
RS-1	36.5	57.8 UO_2, 10.5 ZrO_2, 13.6 Zr, 14.4 Fe, 3.7 Cr	10.0	10.0	2430
RS-2	30	65.0 UO_2, 12.8 ZrO_2, 22.2 Zr	15.0	12.29	2520
RS-3	70	62.2 UO_2, 28.7 ZrO_2, 9.1 Zr	15.0	12.65	2530

Table 11. Summary of Pre/Post Reaction Compositions for Spreading Test RS-0

Constituent	Reactant (wt%)	Product (wt%)	
		Before Mo Segregation	After Mo Segregation
U	34.9	-----	-----
UO_3	14.0	-----	-----
UO_2	-----	52.8	63.5
Zr	25.8	12.9	15.5
ZrO_2	-----	17.5	21.0
MoO_3	25.3	-----	-----
Mo	-----	16.8	-----

while the lower 10 cm of the dam had been melted through, as intended.

Data from the pyrometer mounted over the melt generator region is shown in Figure 17. The peak melt temperature measured by this device corresponds to 2380 C occurring at ~12 seconds, which is ~7 seconds after the spreading transient was over. The absence of a reliable signal up to this point is due to aerosol formation during the burn, which interferes with the measurement. The melt temperature measured 73.7 cm from the dam location is shown in Figure 18. The peak temperature at this location corresponds to 2430 C. This temperature is ~40 C less than the peak melt temperature of 2470 C measured during developmental testing of this chemical mixture (see Figure 19). Thus, the temperature loss during the spreading phase for this test is estimated to be ~40 C.

In general, the corium viscosity for all tests is estimated from the leading edge data using Huppert's solution[2] which relates leading edge penetration to the initial fluid volume, channel width, and viscosity. For the case of 1-D channel flow in which a finite volume of fluid is initially present on the spreading surface at time t = 0 (i.e., the dam break problem), the solution is of the form:

$$L(t) = C\left(\frac{\rho g q^3}{\mu}\right)^{1/5} t^{1/5} \qquad (1)$$

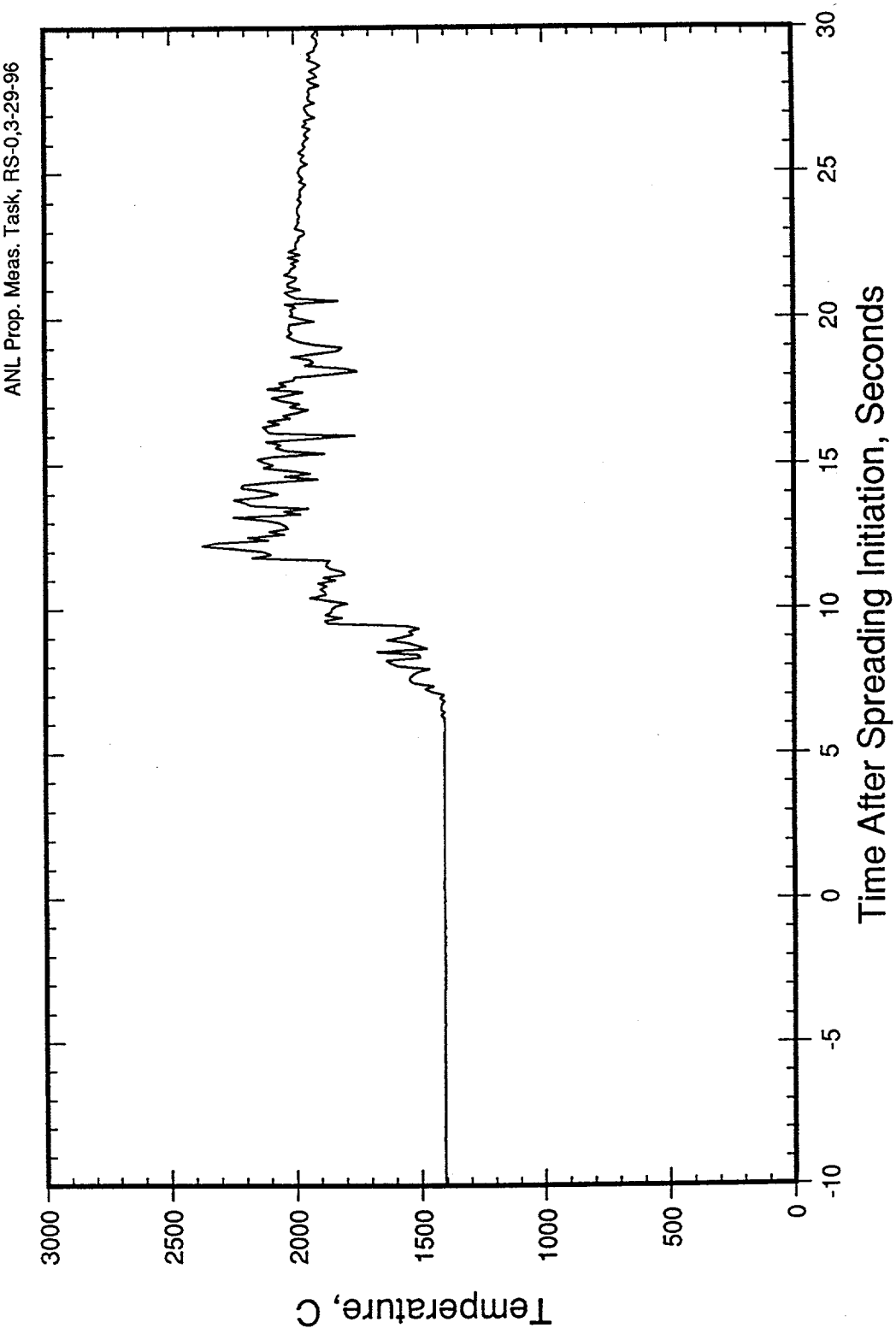

Figure 17. RS-0 Pyrometer Data

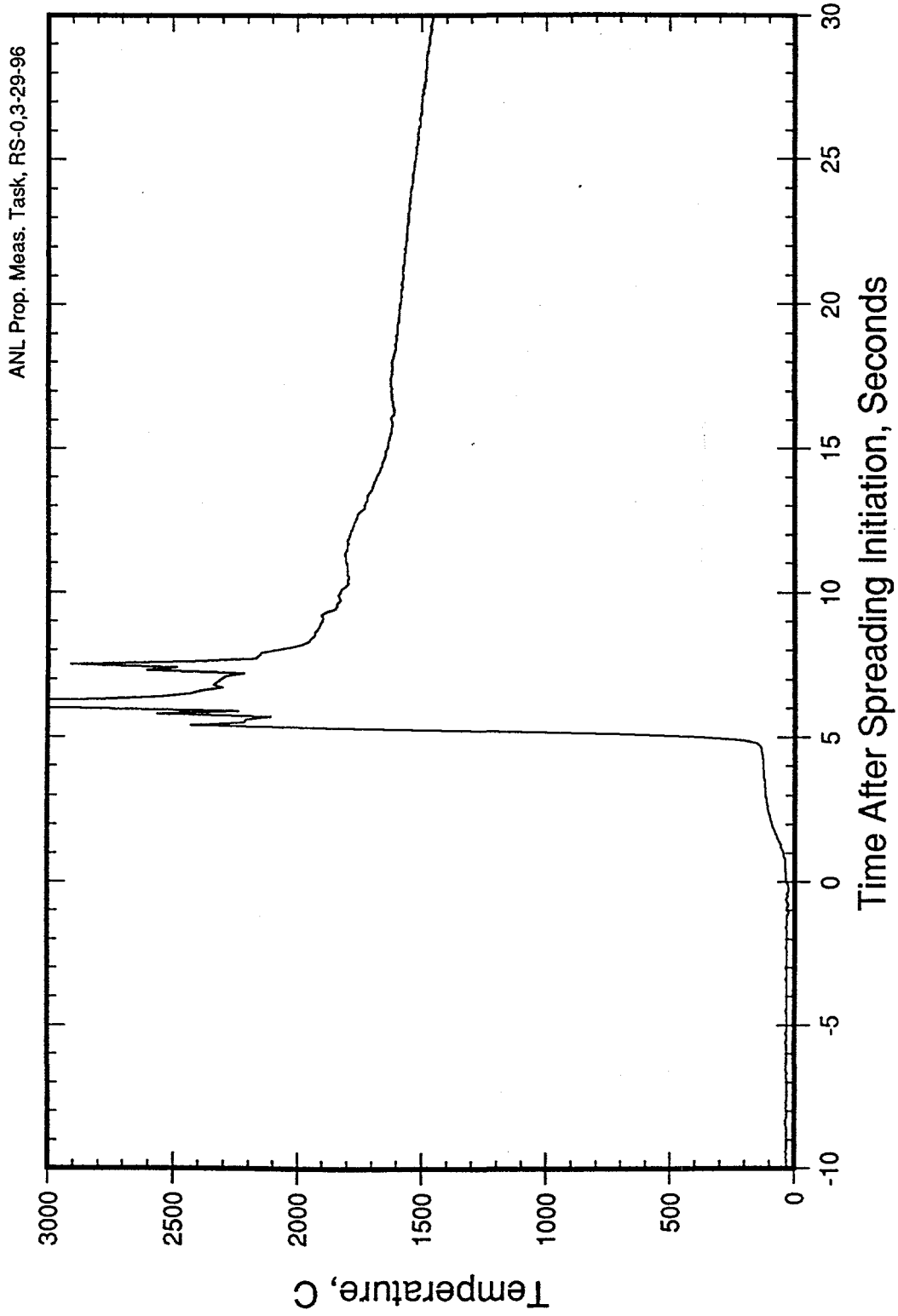

Figure 18. Melt Temperature 73.7 cm from Dam Location for RS-0

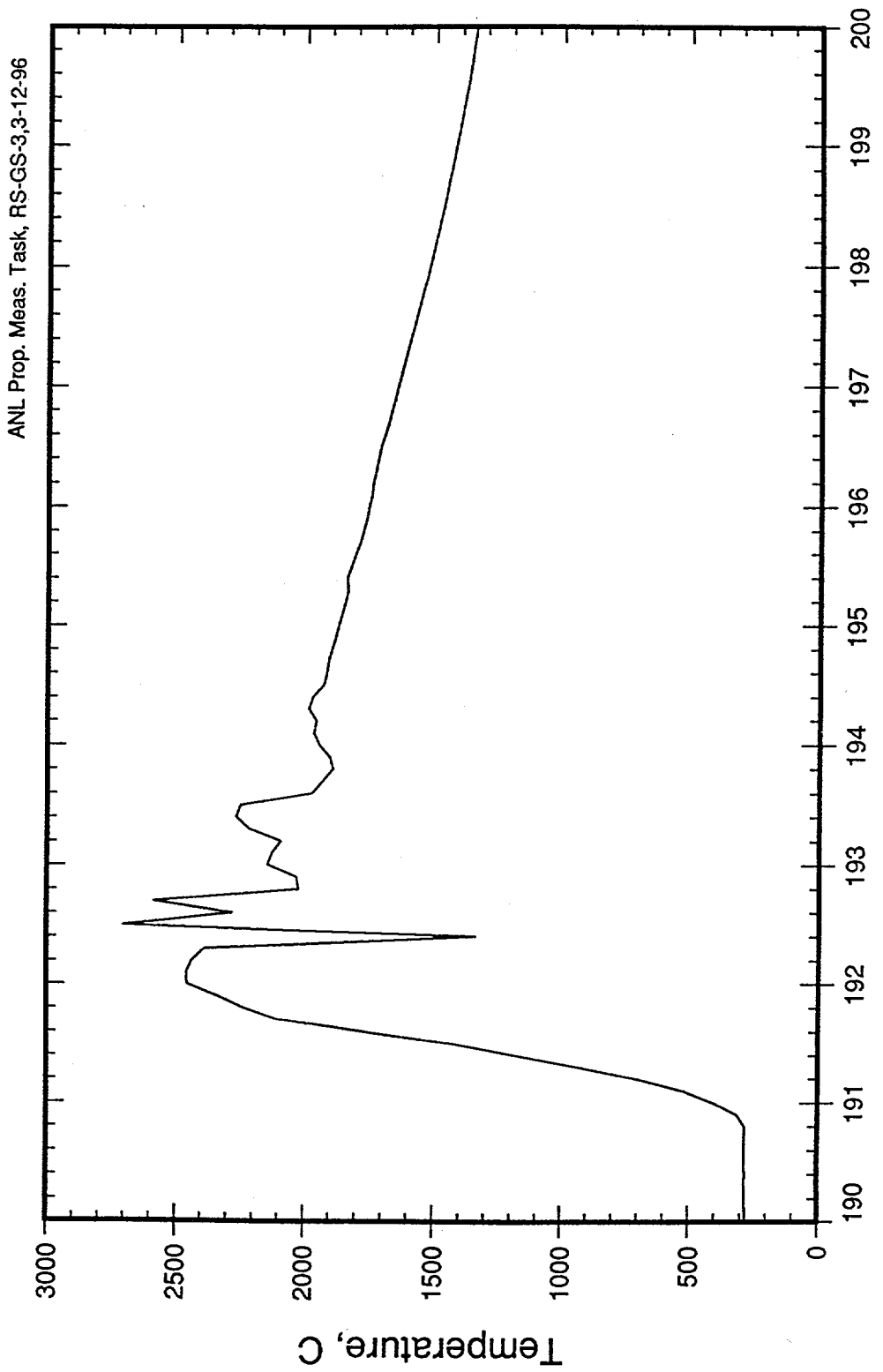

Figure 19. Melt Temperature for RS-0 Thermite Mixture Measured During Developmental Testing

where:

L	=	leading edge penetration,
t	=	time after spreading initiation,
C	=	constant = 1.411....,
g	=	gravitational acceleration,
μ	=	kinematic viscosity,
ρ	=	melt density,
q	=	$m/\rho W$,
m	=	spreading melt mass, and
W	=	channel width = 15.88 cm.

The above equation provides a general relationship between leading edge penetration distance versus time. Huppert also performed an order-of-magnitude scaling analysis to determine the transition time, t_T, at which viscous and inertial forces are comparable. For the above stated set of assumptions, this solution for the transition time reduces to:

$$t_T = \left(\frac{\rho^3 q^4}{g^2 \mu^3} \right)^{1/7}. \qquad (2)$$

For times greater than t_T, viscous forces dominate the flow characteristics, while for times less than this, inertial forces are dominant.

According to Eq. 1, the leading edge penetration varies with time to the 1/5 power after viscous effects begin to dominate the flow characteristics. The leading edge penetration data for RS-0 is plotted in Figure 20 as a function of time after spreading initiation raised to the 1/5 power. After inertial effects have died away, the leading edge penetration should become linear on this plot when viscous effects become dominant. As is evident from the figure, the data do indicate a linear trend for spreading distances greater than 25 cm. In order to estimate the viscosity from this data, a least squares curve fit was performed on the data in Figure 20 for spreading distances greater than 25 cm; the result is shown in the figure. From the slope of this line, the viscosity was back-calculated using Eq. 1, the spreading mass shown in Table 10, and the calculated melt density of 7500 Kg/m^3 for the composition shown in Table 10. The results of this analysis are summarized as

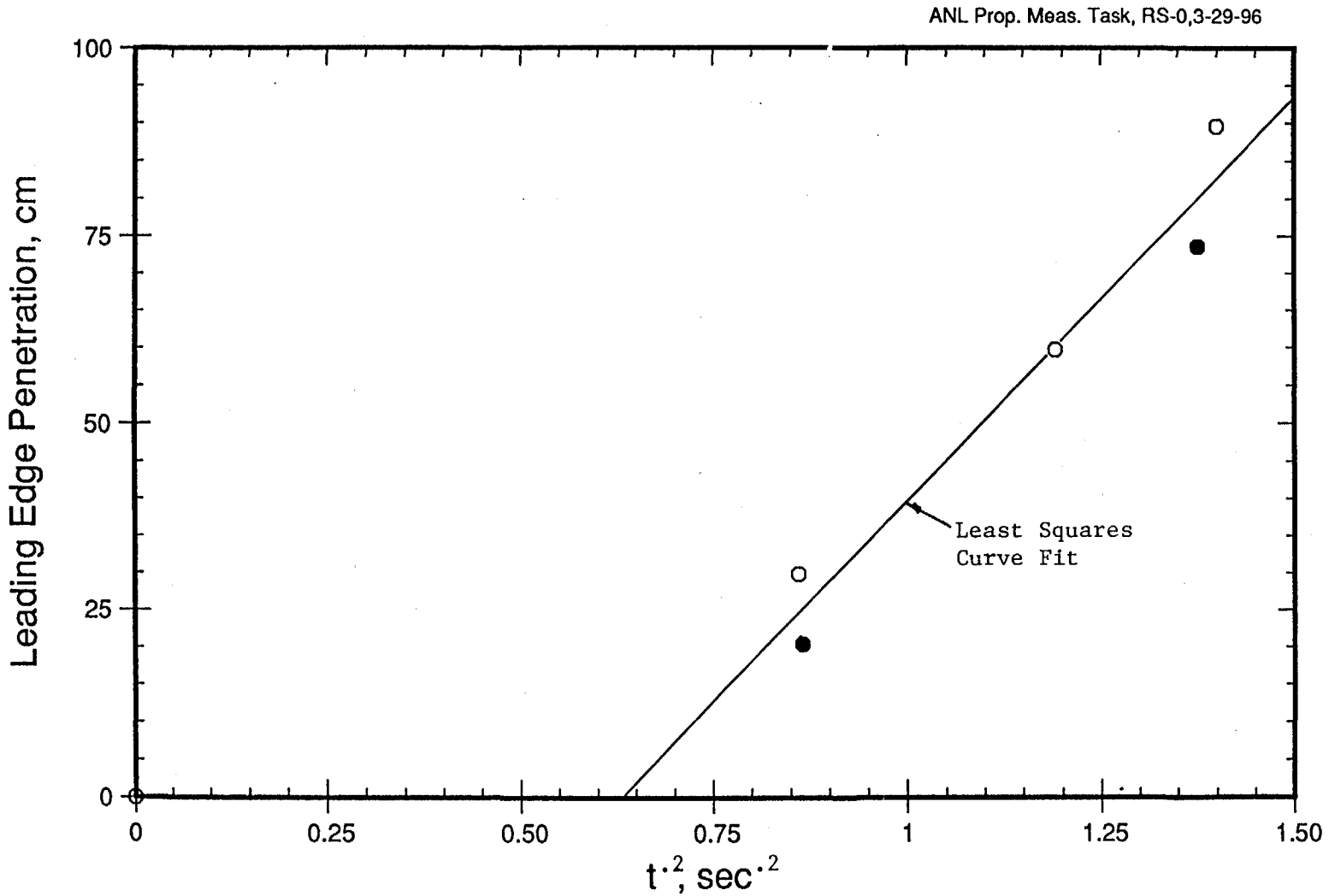

Figure 20. RS-0 Melt Leading Edge Location Plotted Versus $t^{1/5}$

follows. The slope of the penetration curve is found to be 107.6 cm/sec$^{1/5}$. The error variance in the slope determination is calculated to be 13.3 cm/sec$^{1/5}$ (see Reference 7, pg. 96 for a description of the methodology used to determine the error estimate). Given this data, the best-estimate of the viscosity for 50% oxidized corium at an initial temperature of 2470 C is calculated to be 113 centipoise (cp), with the uncertainty range being 64-212 cp. A final check on the applicability of this model for the determination of the corium viscosity in this test is provided by Eq. 2. From this equation, the transition time at which viscous forces begin to dominate the flow characteristics is evaluated as ~4 seconds given the best estimate viscosity and other input data described above. From Figure 16, the overall duration of the spreading transient is noted to be ~ 6 seconds, which is longer than the predicted transition time. However, as described by Huppert, the analysis underlying Eq. 2 is order-of-magnitude; the data shown in Figures 16 and 20 seem to indicate viscous-dominated flow for times greater than ~1 second.

During posttest examinations, the solidified debris depth was measured as a function of spreading distance at the centerline of the channel. The data is provided in Figure 21 for spreading model validation purposes. The mass of Mo metal recovered from the melt generator region for test RS-0 is shown in Table 12. The recovered mass corresponds to 780 g, which corresponds to 31%

Table 12. Recovered Mo Mass from Spreading Tests

Test	Mass Mo Recovered (Kg)	Theoretical Mo Mass (Kg)	Mass Removed/ Theoretical Mass
RS-0	0.78 ± 0.08	2.52	0.309
RS-2	4.01 ± 0.4	2.72	1.47
RS-3	2.94 ± 0.3	2.36	1.25

of the initial Mo present (see Table 11). This was the lowest recovery fraction for the three tests in which Mo was generated as a reaction byproduct. The estimated error of 10% in the recovery mass is based on the fact that the oxide and metal were partially bonded together, and a complete separation of the two phases in the melt generator region was not possible.

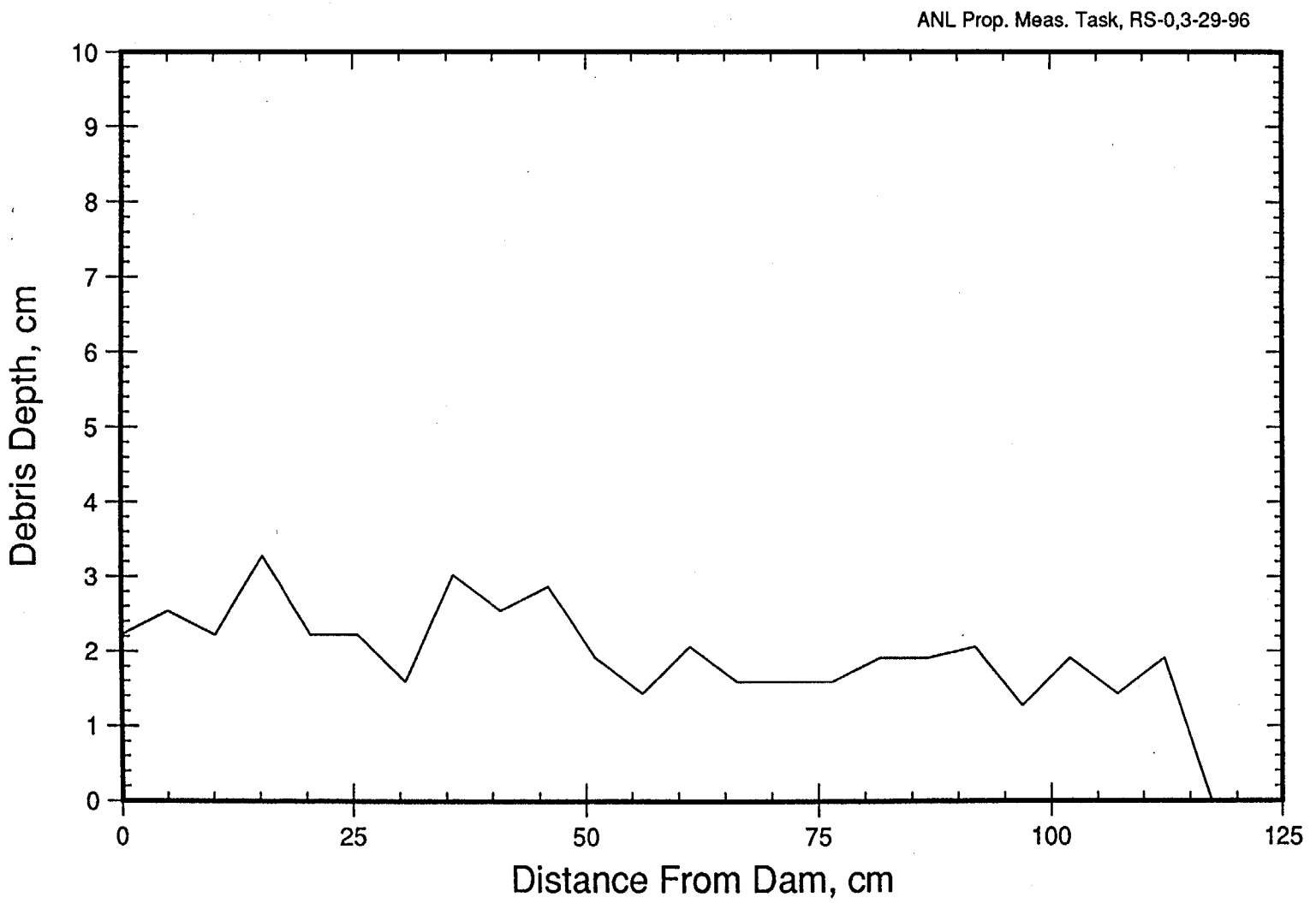

Figure 21. RS-0 Posttest Debris Distribution

The second test conducted in the series, RS-1, utilized 36% oxidized corium containing 18 wt % stainless steel. The pre- and post-reaction compositions for this test are shown in Table 13. The voltage signals from the burn wires are shown in Figure 22. The location of the melt leading edge after initiation of spreading, as deduced from the burn wire data, is shown in Figure 23. The melt arrival times in this figure have been shifted such that t = 0 corresponds to the onset of spreading, as indicated by the data from the burn wire located at the dam surface (see Figure 14). The test data (see Figure 23), in conjunction with posttest examination of the debris and video footage from the test, indicated that some of the melt had breached the upper portion of the dam prior to failure of the lower meltthrough barrier, which initiated the full-scale spreading transient. A rough estimate of the melt mass which breached the upper portion of the dam is 1 Kg, which corresponds to 10% of the initial melt mass. This rough estimate is based on video footage from the experiment. This initial loss of melt is factored into the error assessment for the viscosity calculation described below.

Table 13. Summary of Pre/Post Reaction Compositions for Spreading Test RS-1

Constituent	Reactant (wt%)	Product (wt%)
U	50.9	-----
UO_2	-----	57.8
Zr	21.5	13.6
ZrO_2	-----	10.5
Fe_2O_3	20.5	-----
Fe	-----	14.4
CrO_3	7.1	-----
Cr	-----	3.7

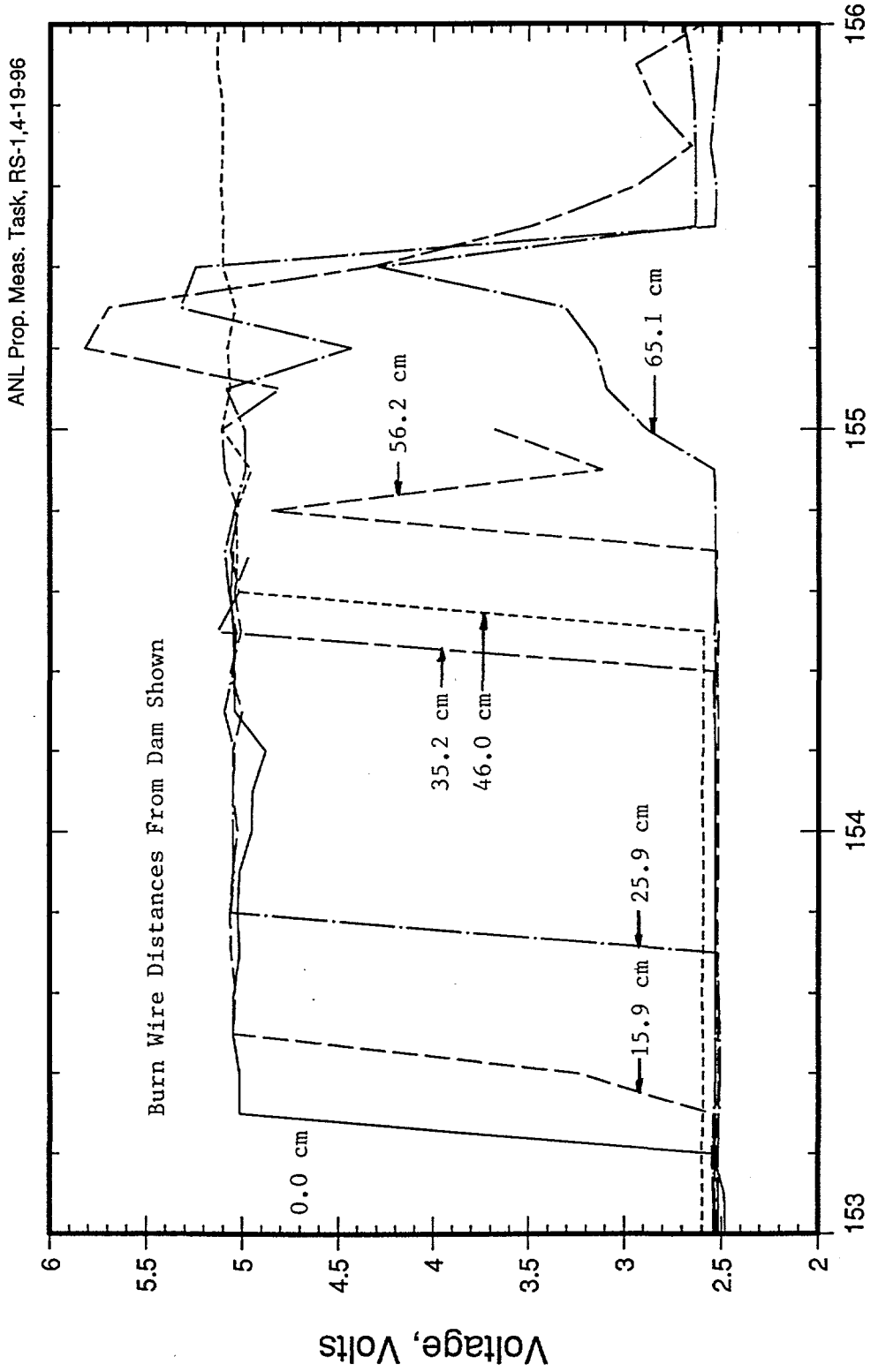

Figure 22. RS-1 Burn Wire Data

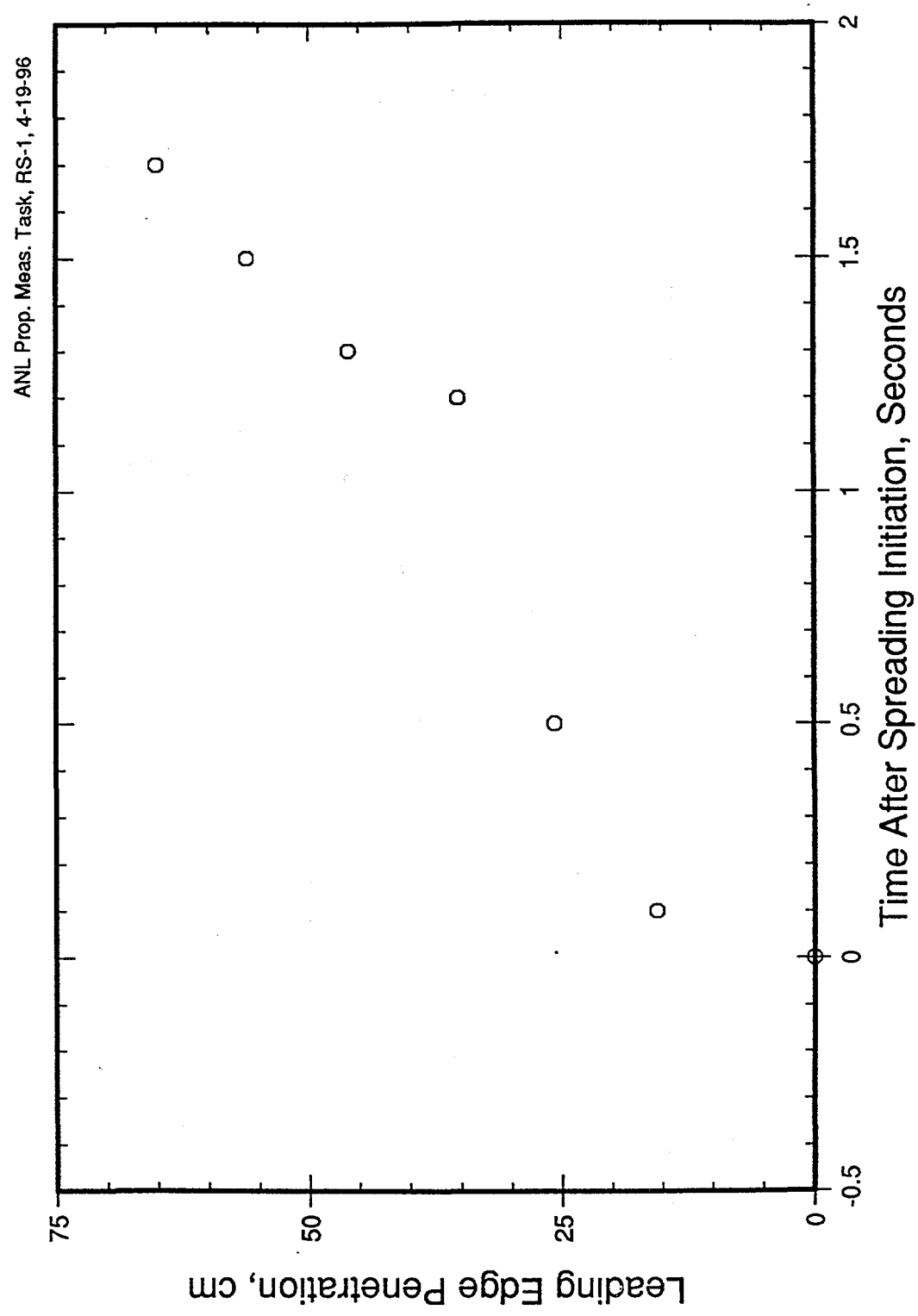

Figure 23. RS-1 Melt Leading Edge Location Versus Time

Data from the pyrometer mounted over the melt generator region is shown in Figure 24. The peak melt temperature measured by this device corresponds to 2350 C occurring just prior to the onset of spreading. This temperature reasonably agrees with sustained signals from the pyrometer after the spreading transient was completed and aerosols had cleared from the plenum of the test section (i.e., t > 3 seconds, at which time temperatures fluctuated up to 2300 C). Thus, the initial melt temperature measurement of 2350 C is deemed to be reliable, and is also in agreement with temperature measurements of 2320-2520 C obtained during development of this chemical mixture[8]. The melt contacted two Type C thermocouples distributed along the length of the channel during the transient, but both these thermocouples failed prior to reaching a plateau. Thus, a direct measurement of the melt temperature loss during spreading was not obtained. However, based on the temperature decline measured by the pyrometer in the generator region over the time interval 0-3 seconds, a lower bound estimate of 50 C is deduced.

The leading edge penetration data for RS-1 is plotted in Figure 25 as a function of time after spreading initiation raised to the 1/5 power. As is evident from the figure, the data indicate a somewhat linear trend for spreading distances greater than 25 cm, as predicted by theory. However, the trend is not as clear in comparison to the other spreading tests which were conducted, which may in part be attributable to premature melt release into the spreading channel, as summarized above. In order to estimate the viscosity from this data, a least squares curve fit was performed on the data in Figure 20 for spreading distances greater than 25 cm; the result is shown in the figure. From the slope of this line, the viscosity was back-calculated using Eq. 1, the spreading mass shown in Table 10, and the calculated melt density of 7540 Kg/m^3 for the composition shown in Table 10. The results of this analysis indicate that the slope of the penetration curve is 148.2 $cm/sec^{1/5}$, with an error variance of 44.8 $cm/sec^{1/5}$. Given this data, the best-estimate of the viscosity for 36% oxidized corium containing 18 wt % stainless steel at an initial temperature of 2350 is 11.2 cp, with an uncertainty range of 2.2 - 68.1 cp. The 10% loss of melt prior to initiation of the full scale spreading transient has been factored into this estimate. This occurrence basically lowers the lower-bound viscosity estimate by ~30%. Note that the best estimate for the viscosity of this corium composition (11.2 cp) is slightly higher than the nominal value normally cited for molten UO_2 (~4.3 cp at 3120 K; see Reference 9). For reference, the order-of-magnitude estimate of the transition time between inertial and viscous-dominated spreading regimes is calculated to be 10 seconds for this test (see

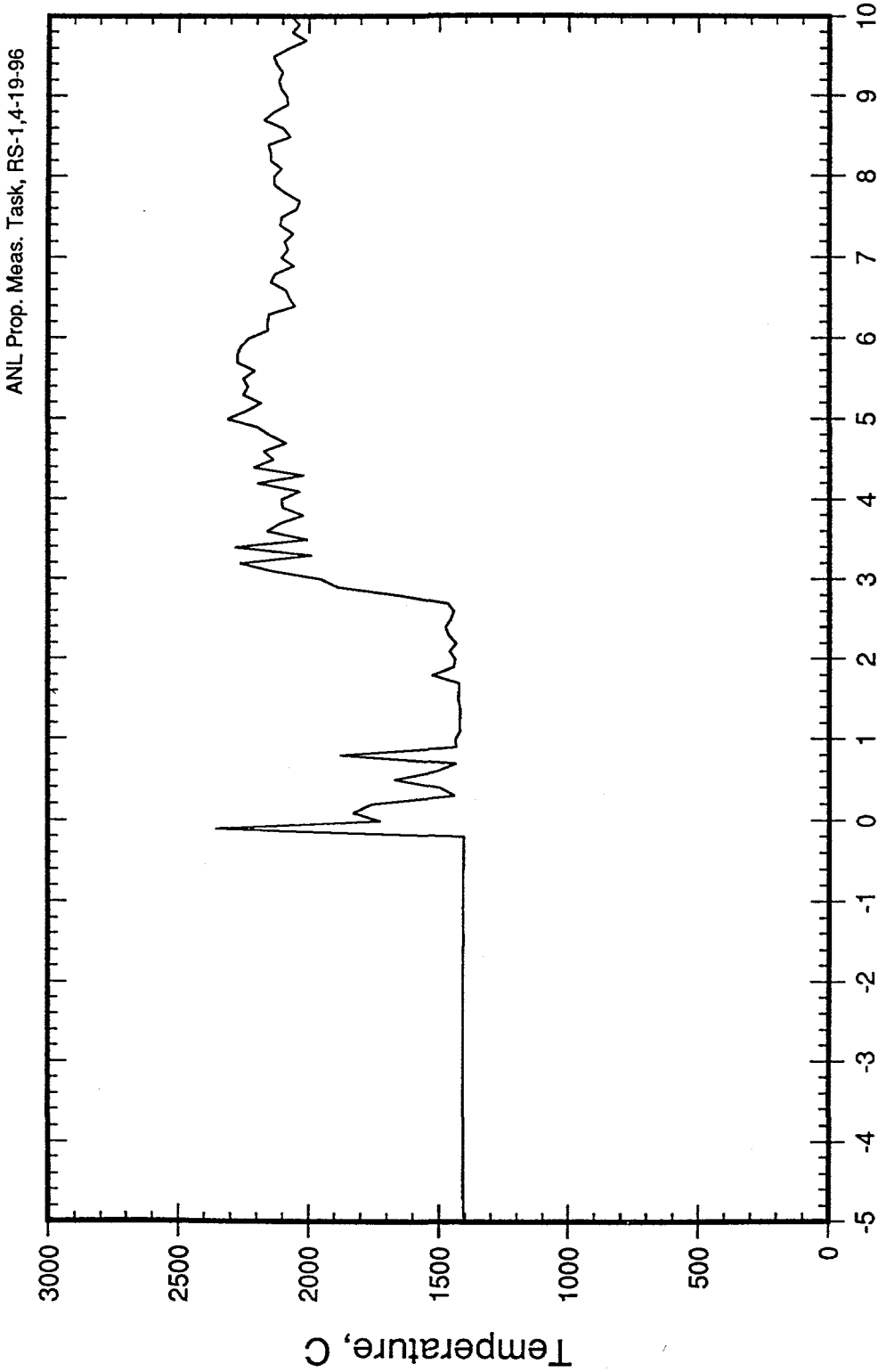

Figure 24. RS-1 Pyrometer Data

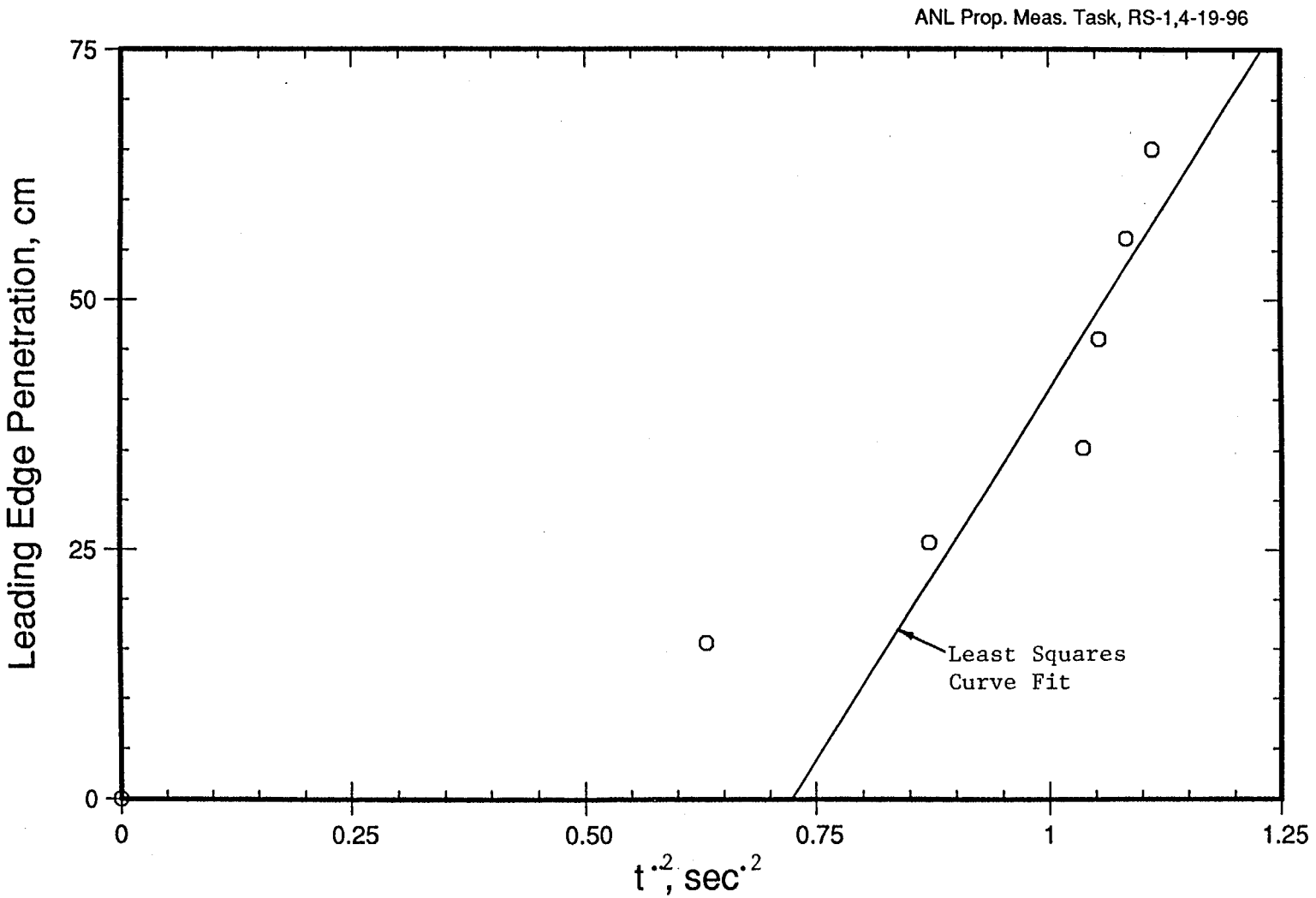

Figure 25. RS-1 Melt Leading Edge Location Plotted Versus $t^{1/5}$

Eq. 2) given the best-estimate viscosity and other data described above. Thus, the 10 second estimated transition time exceeds the actual spreading time of nominally 2 seconds. However, the data from this experiment seem to roughly obey the governing equation for viscous-dominated spreading (see Eq. 1 and Figure 25). Moreover, the viscosity estimated using this approach is in-line with other high-temperature oxide data (see Reference 9).

During posttest examinations, the solidified debris depth was measured as a function of spreading distance at the centerline of the channel. The data is provided in Figure 26 for spreading model validation purposes. Mo metal was not generated as a reaction by-product in this experiment. In terms of the free metals present in the reaction byproducts (i.e., Zr and molten and stainless steel), these materials were intimately intermixed with the oxide phase; i.e., no phase segregation was observed over the timescale of the spreading transient, nor during the posttest cooldown.

The third test conducted in the series, RS-2, utilized 30% oxidized corium. The pre- and post-reaction compositions for this test are shown in Table 14. The voltage signals from the burn wires are shown in Figure 27. The location of the melt leading edge after initiation of spreading, as deduced from the burn wire data, is shown in Figure 28. The melt arrival times in this figure have been shifted such that t = 0 corresponds to the onset of spreading, as indicated by the data from the burn wire located at the dam surface (see Figure 14). The test data (see Figure 28) seem to indicate that some of the melt had breached the upper portion of the dam prior to failure of the lower meltthrough barrier, as occurred in test RS-1. However, upon posttest examination of the debris, the upper portion of the dam was found to be intact, as intended. Examination of the video footage indicated that melt droplets were ejected over the top of the dam prior to initiating the spreading transient, which may have lead to spurious deflection of the first two burn wires. The estimated mass which was distributed in droplet form prior to initiation of the spreading transient is << 1%; this occurrence is therefore neglected in the viscosity assessment.

Data from the pyrometer mounted over the melt generator region is shown in Figure 29. The peak melt temperature measured by this instrument fluctuated around 2520 C beginning ~13 seconds after spreading was initiated; the absence of a signal up to this time is due to aerosols present in the plenum of the test section. Since the Type C thermocouple located in the melt generator region failed prior to reaching a plateau, the sustained reading of 2520 C recorded by the pyrometer is taken as a lower bound estimate of the melt temperature at start of the spreading transient. Data obtained

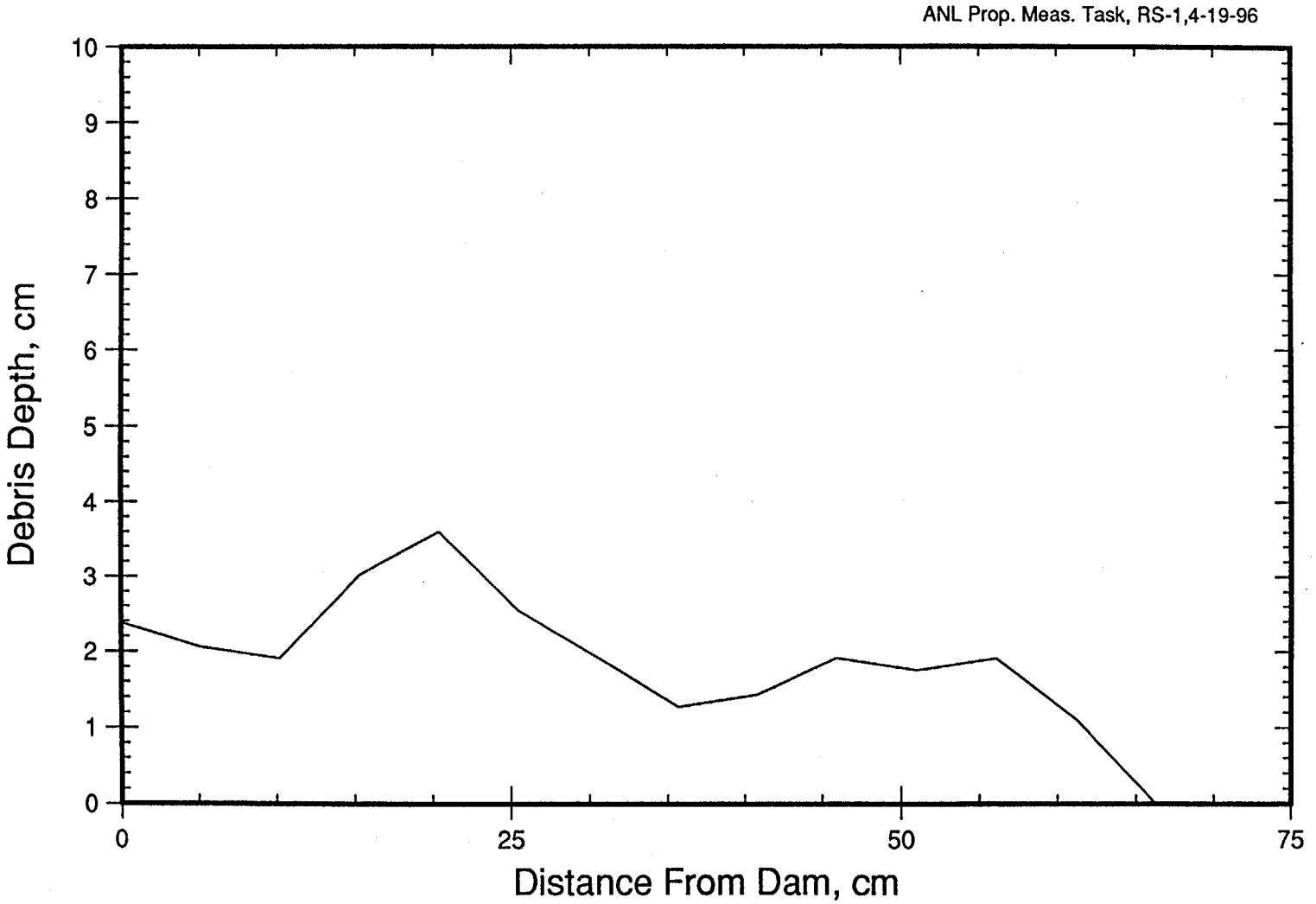

Figure 26. RS-1 Posttest Debris Configuration

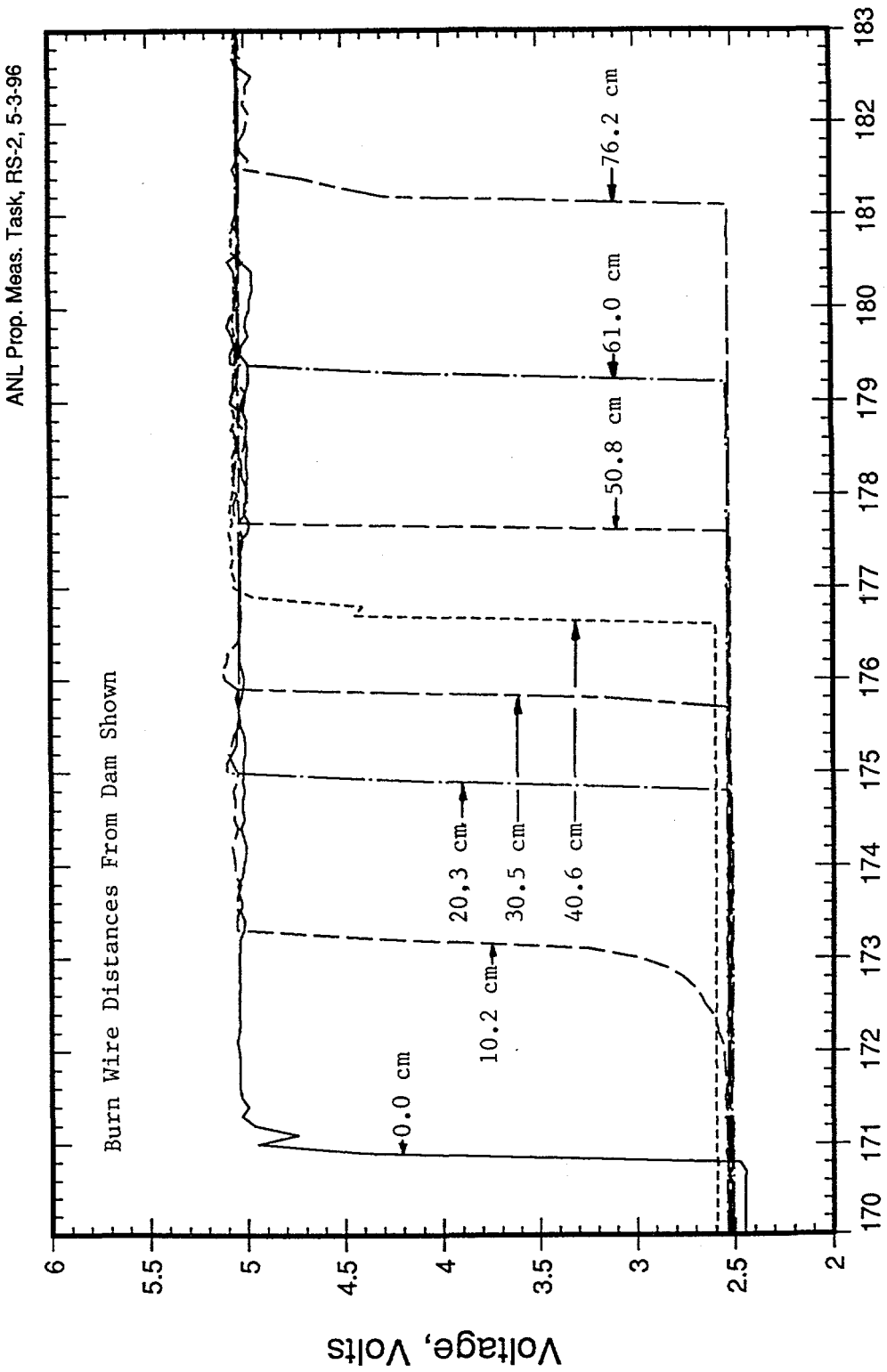

Figure 27. RS-2 Burn Wire Data

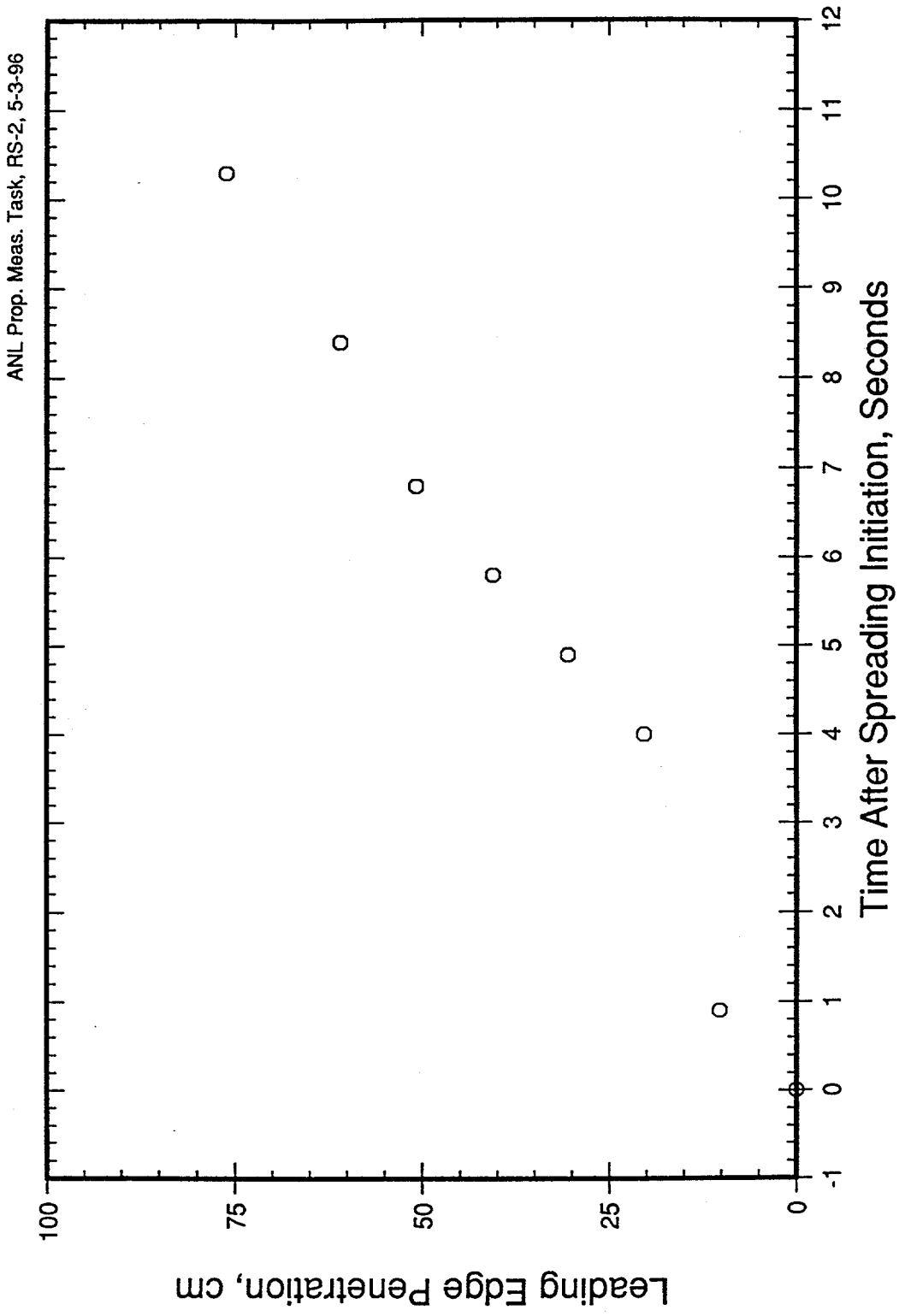

Figure 28. RS-2 Melting Leading Edge Location Versus Time

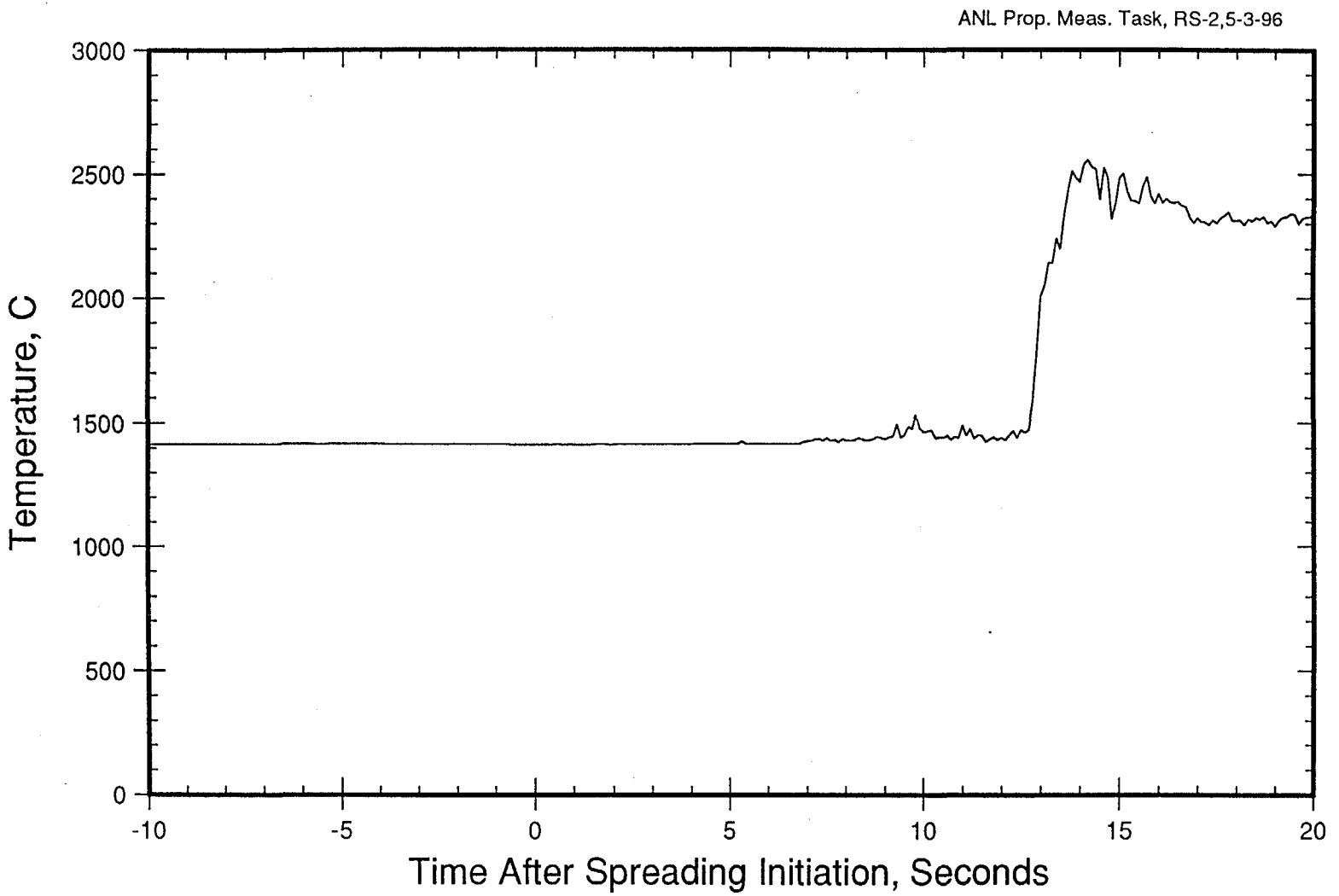

Figure 29. RS-2 Pyrometer Data

Table 14. Summary of Pre/Post Reaction Compositions for Spreading Test RS-2

Constituent	Reactant (wt%)	Product (wt%)	
		Before Mo Segregation	After Mo Segregation
U	46.9	-----	-----
UO_3	-----	-----	-----
UO_2	-----	53.2	65.0
Zr	26.0	18.2	22.2
ZrO_2	-----	10.6	12.8
MoO_3	27.1	-----	-----
Mo	-----	18.1	-----

from the second Type C thermocouple located 20.3 cm from the dam is shown in Figure 30. As is evident, this thermocouple recorded a temperature of ~2000 C at t = 5 seconds before failing as the temperature was still rising. After this time, it appears as though a false junction formed near t = 9 seconds, at which time the temperature was nominally 2480 C. However, the location of the junction is uncertain. In lieu of additional data, the temperature loss of the melt during the spreading phase is estimated as ~ 40 C during this test, which is approximately the same temperature loss estimated for the previous two tests.

The leading edge penetration data for RS-2 is plotted in Figure 31 as a function of time after spreading initiation raised to the 1/5 power. As is evident from the figure, the data for spreading distances greater than 10 cm indicate a very linear relationship, in agreement with the viscous flow theory. The least-squares curve fit to this data is shown on the plot. From the slope of this line, the viscosity was back-calculated using Eq. 1, the spreading mass shown in Table 10, and the calculated melt density of 7550 Kg/m^3 for the composition shown in Table 10. The results of this analysis indicate that the slope of the penetration curve is 202.7 $cm/sec^{1/5}$, with an error variance of 5.1 $cm/sec^{1/5}$. Given this data, the best-estimate of the viscosity for 30% oxidized corium at an initial

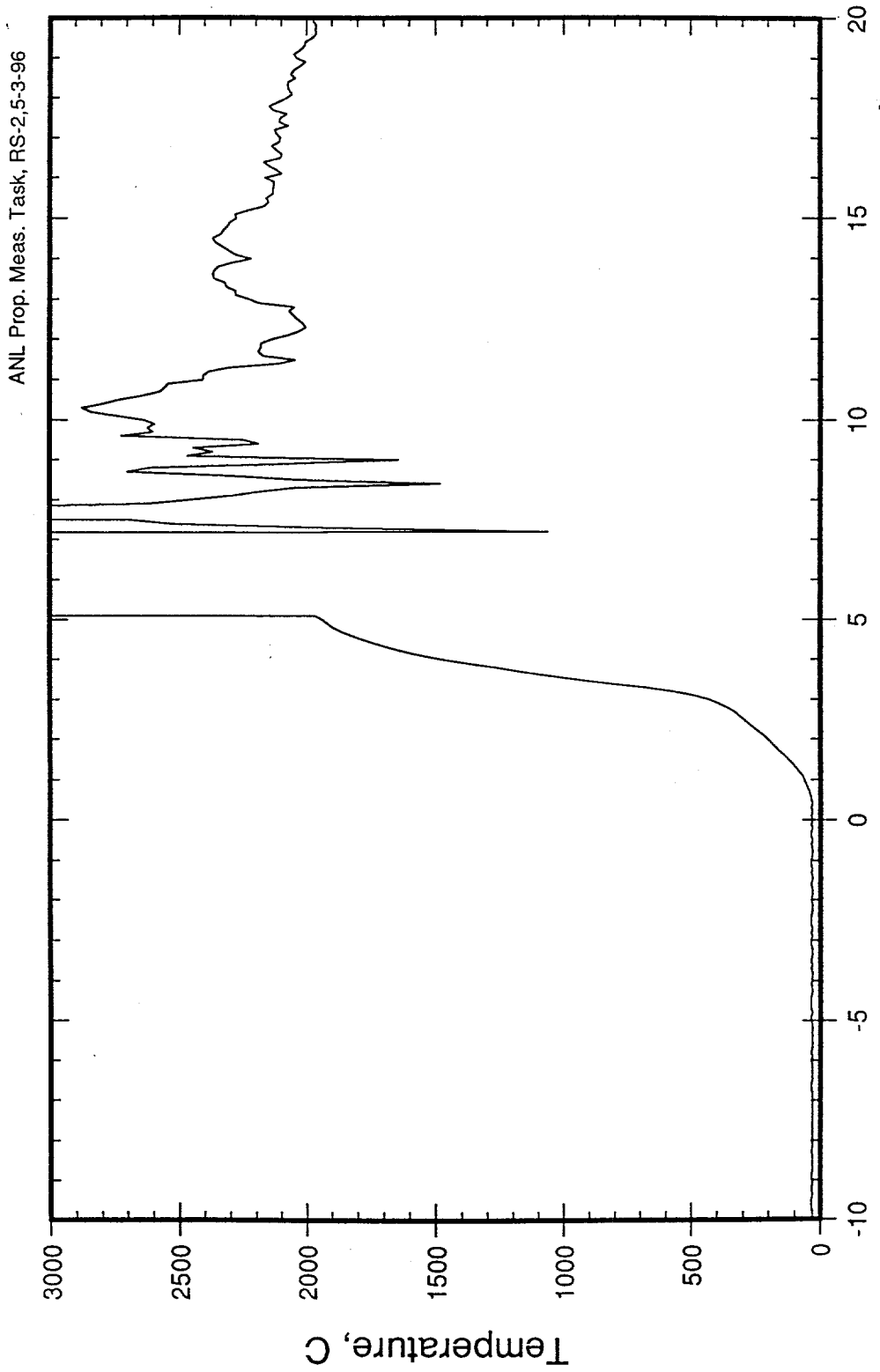

Figure 30. Melt Temperature 20.3 cm from Dam Location for RS-2

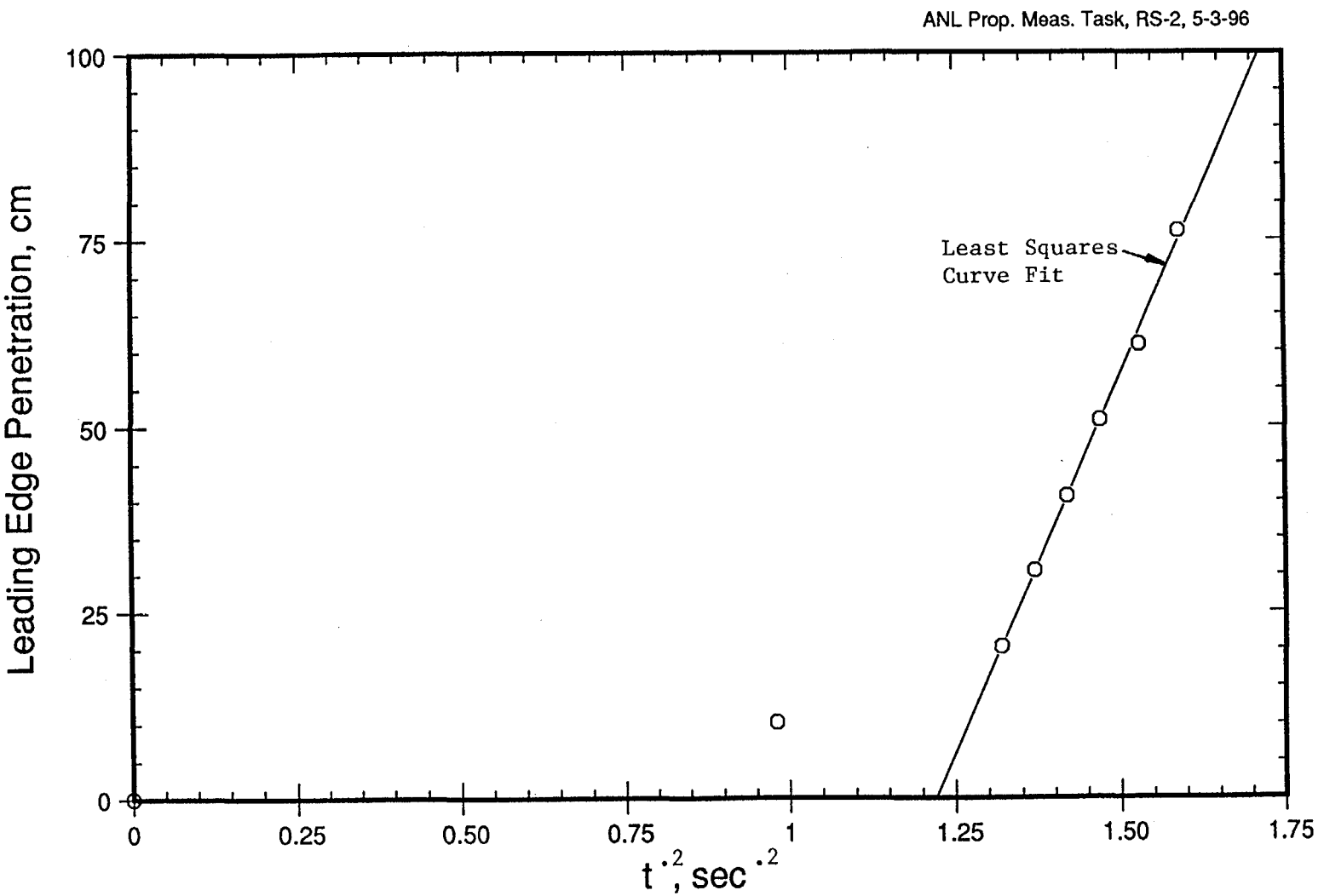

Figure 31. RS-2 Melt Leading Edge Location Plotted Versus $t^{1/5}$

temperature of 2520 C is 4.4 cp, with an uncertainty range of 3.8 - 5.0 cp. Note that the best estimate for the viscosity of this corium composition (4.4 cp) is virtually the same as the value cited for molten UO2 (~4.3 cp at 3120 K; see Reference 9). For reference, the order-of-magnitude estimate of the transition time between inertial and viscous-dominated spreading regimes is calculated to be 17 seconds for this test (see Eq. 2) given the best-estimate viscosity and other data described above. Thus, the 17 second estimated transition time exceeds the actual spreading time of nominally 12 seconds. However, the data from this experiment seem to clearly obey the governing equation for viscous-dominated spreading for spreading distances greater than 20 cm (see Eq. 1 and Figure 30). Moreover, the viscosity estimated using this approach is in-line with other high-temperature oxide data (see Reference 9).

During posttest examinations, the solidified debris depth was measured as a function of spreading distance at the centerline of the channel. The data is provided in Figure 32 for spreading model validation purposes. The mass of Mo metal recovered from the melt generator region for test RS-2 is shown in Table 12. The recovered mass exceeds the theoretical Mo mass by 47% (see Table 14). As described previously, this measurement was difficult to make accurately due to the fact that the metal and oxide were partially bonded together at the interface, making separation of the two materials difficult during posttest disassembly.

The fourth test conducted in the series, RS-3, utilized 70% oxidized corium. The pre- and post-reaction compositions for this test are shown in Table 15. The voltage signals from the burn

Table 15. Summary of Pre/Post Reaction Compositions for Spreading Test RS-3

Constituent	Reactant (wt%)	Product (wt%)	
		Before Mo	After Mo
U	23.1	-----	-----
UO_3	27.8	-----	-----
UO_2	-----	52.4	62.2
Zr	25.6	7.7	9.1
ZrO_2	-----	24.2	28.7
MoO_3	23.5	-----	-----
Mo	-----	15.7	-----

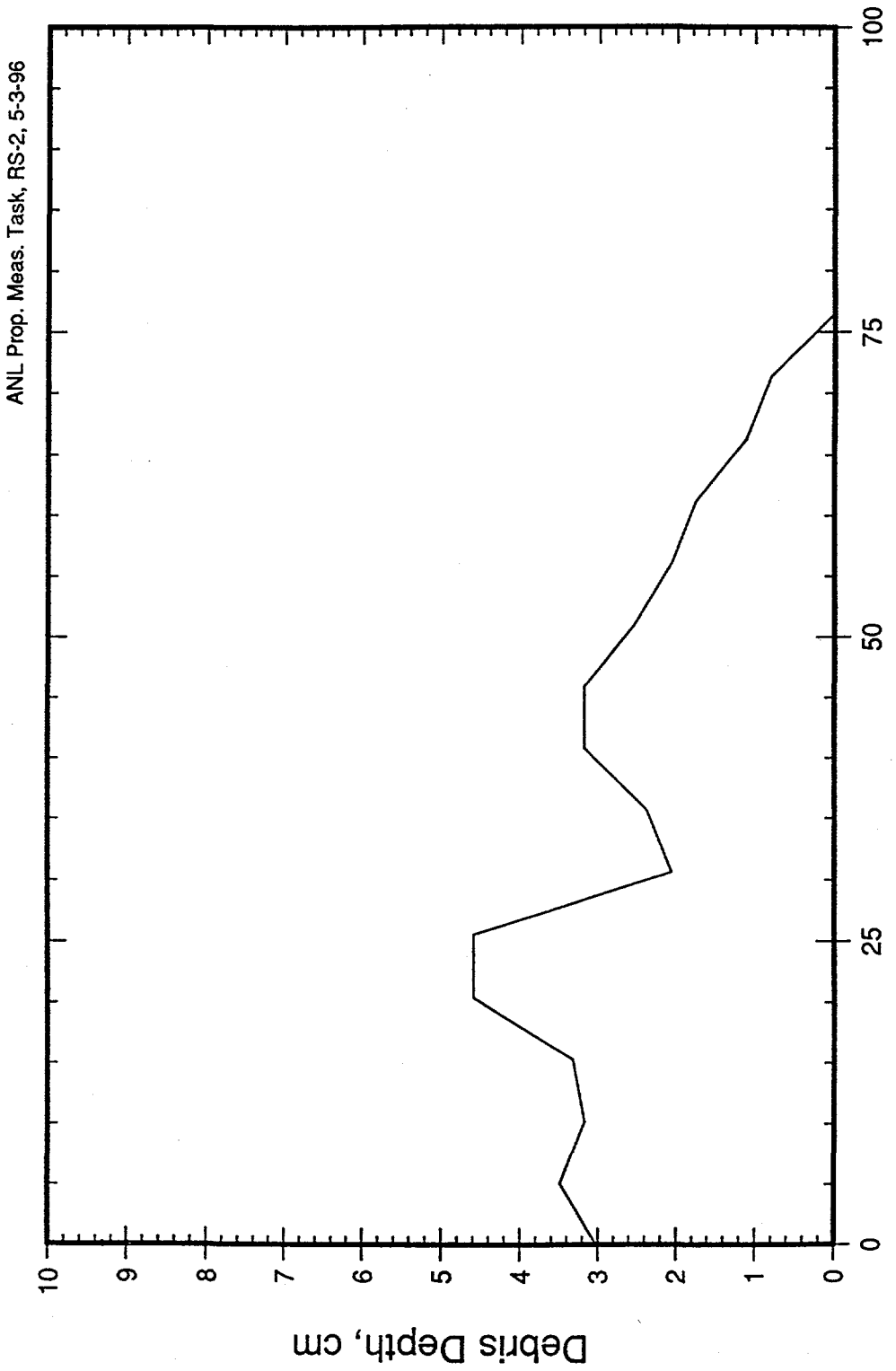

Figure 32. RS-2 Posttest Debris Configuration

wires are shown in Figure 33. The location of the melt leading edge after initiation of spreading, as deduced from the burn wire data, is shown in Figure 34. The melt arrival times in this figure have been shifted such that t = 0 corresponds to the onset of spreading, as indicated by the data from the burn wire located at the dam surface (see Figure 14). The test data, in conjunction with posttest examinations, indicated that the dam design worked as intended in this experiment.

Data from the pyrometer mounted over the melt generator region is shown in Figure 35. The peak melt temperature corresponds to 2150 C, and occurs ~14.5 seconds after spreading initiation (or ~4 seconds after spreading terminated; see Figure 34). As discussed below, this measurement is significantly lower than those recorded by Type C thermocouples located along the length of the spreading surface, which is most likely attributable to aerosol generation during the spreading phase. The melt temperature measurements recorded at 20.3 and 45.7 cm from the dam are shown in Figures 36 and 37, respectively. The peak temperature recorded at the 20.3 cm location is noted to be 2530 C, while at the 45.7 cm location, the peak temperature corresponds to 2600 C. Obviously, the melt temperature should not increase as the melt spreads, particularly since exothermic chemical reactions were not active during this test. Thus, 2530 C is adopted as the best estimate for the melt temperature, with temperature loss by the melt during the spreading transient estimated to be very low (<10 C). Note that the reported accuracy of these thermocouples is 1% under ideal conditions in the temperature range under consideration. Thus, the discrepancy between the two readings is almost bounded by the error range for the thermocouples.

The leading edge penetration data for RS-3 is plotted in Figure 38 as a function of time after spreading initiation raised to the 1/5 power. As is evident from the figure, the data for spreading distances greater than 10 cm indicate a fairly linear relationship, but there is evidence of a slight curvature in the data. This could be due to temperature effects, which were previously judged to be minor in this experiment, or an indication of non-ideal viscous flow behavior (i.e., Non-Newtonian affects). The least-squares curve fit to this data is shown on the plot. From the slope of this line, the viscosity was back-calculated using Eq. 1, the spreading mass shown in Table 10, and the calculated melt density of 7460 Kg/m^3 for the composition shown in Table 10. The results of this analysis indicate that the slope of the penetration curve is 50.5 $cm/sec^{1/5}$, with an error variance of 7.0 $cm/sec^{1/5}$. Given this data, the best-estimate of the viscosity for 70% oxidized corium at an initial temperature of 2530 C is 5070 cp, with an uncertainty range of 2650-10700 cp. For reference, the

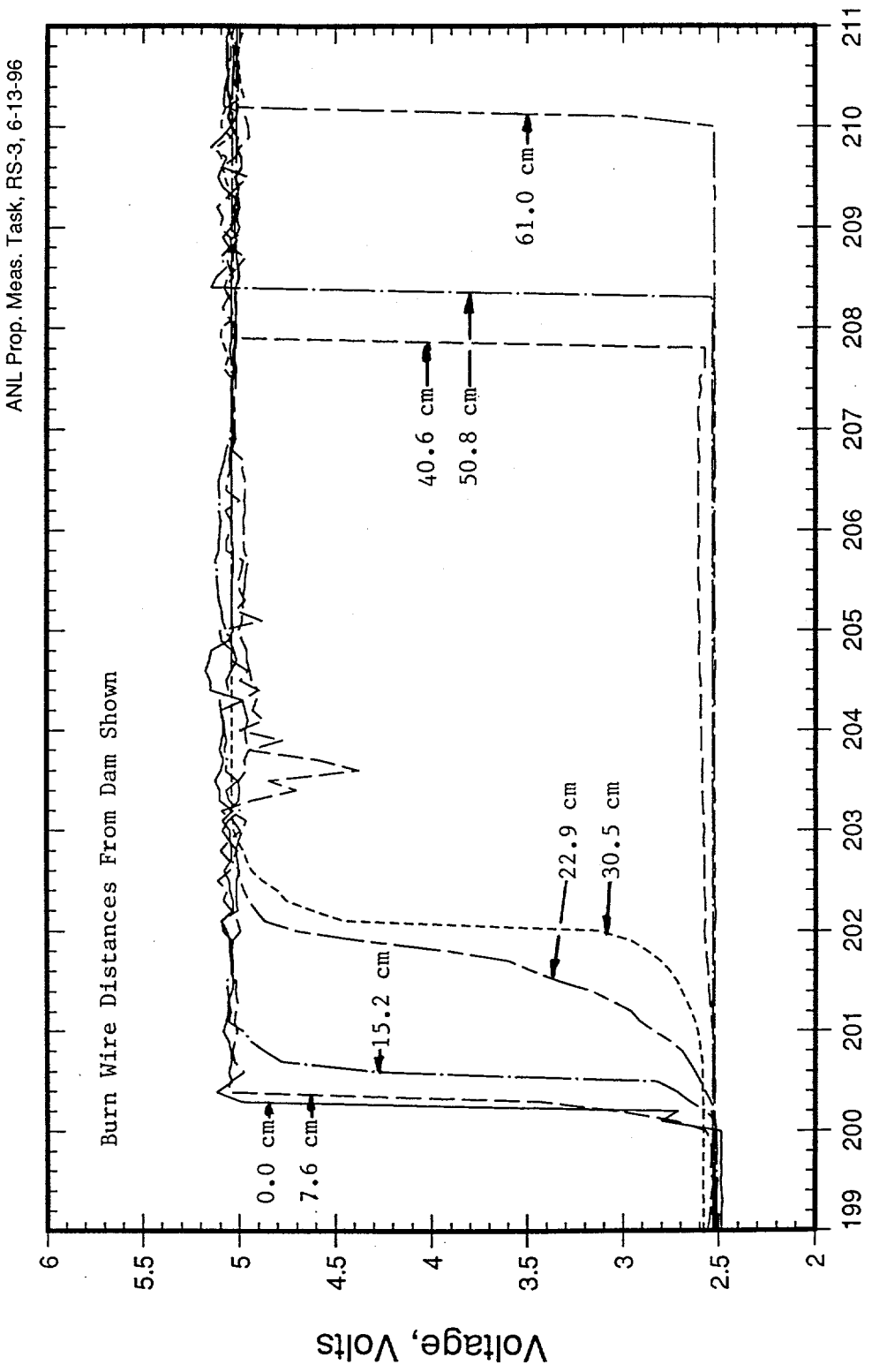

Figure 33. RS-3 Burn Wire Data

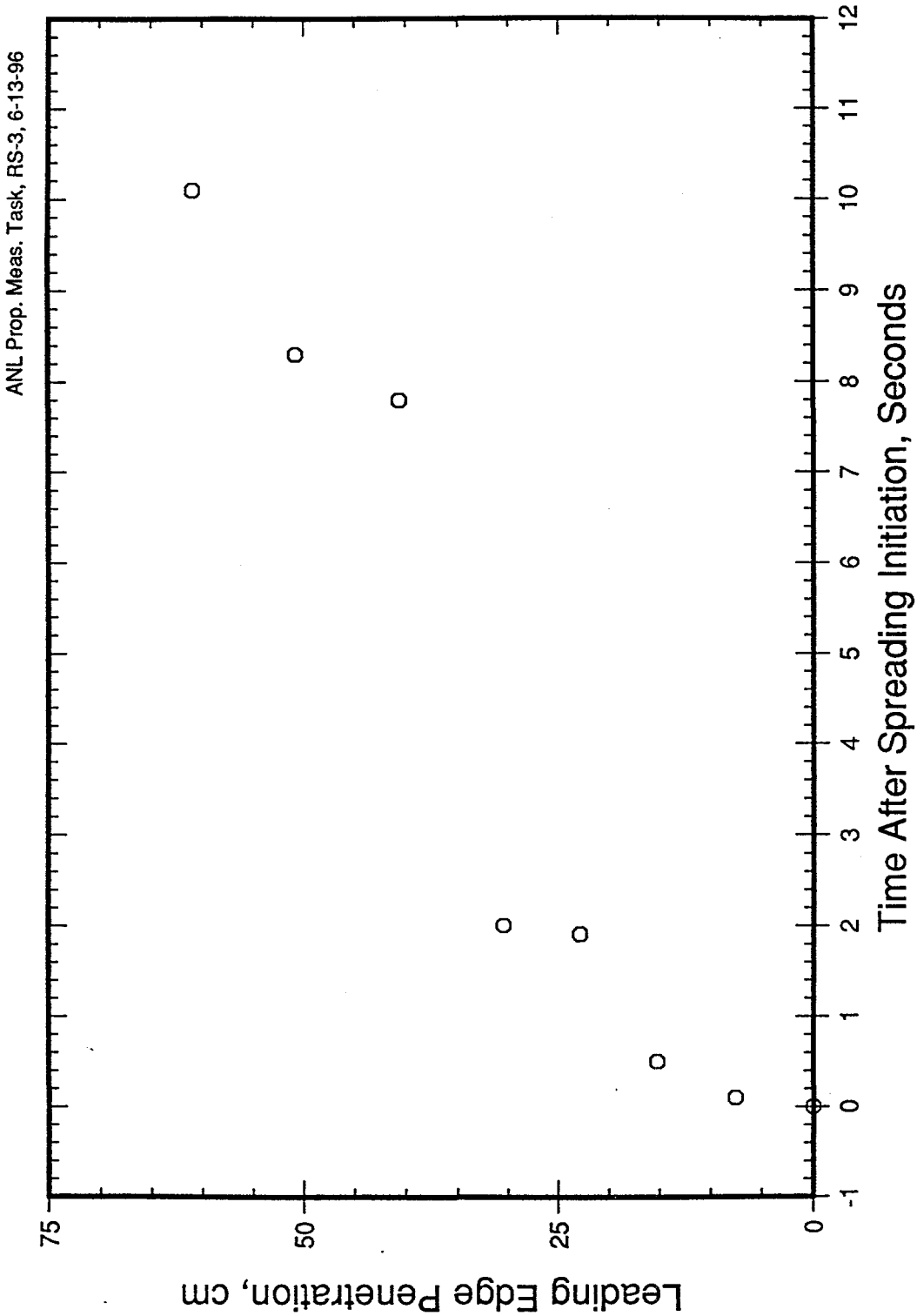

Figure 34. RS-3 Melt Leading Edge Location Versus Time

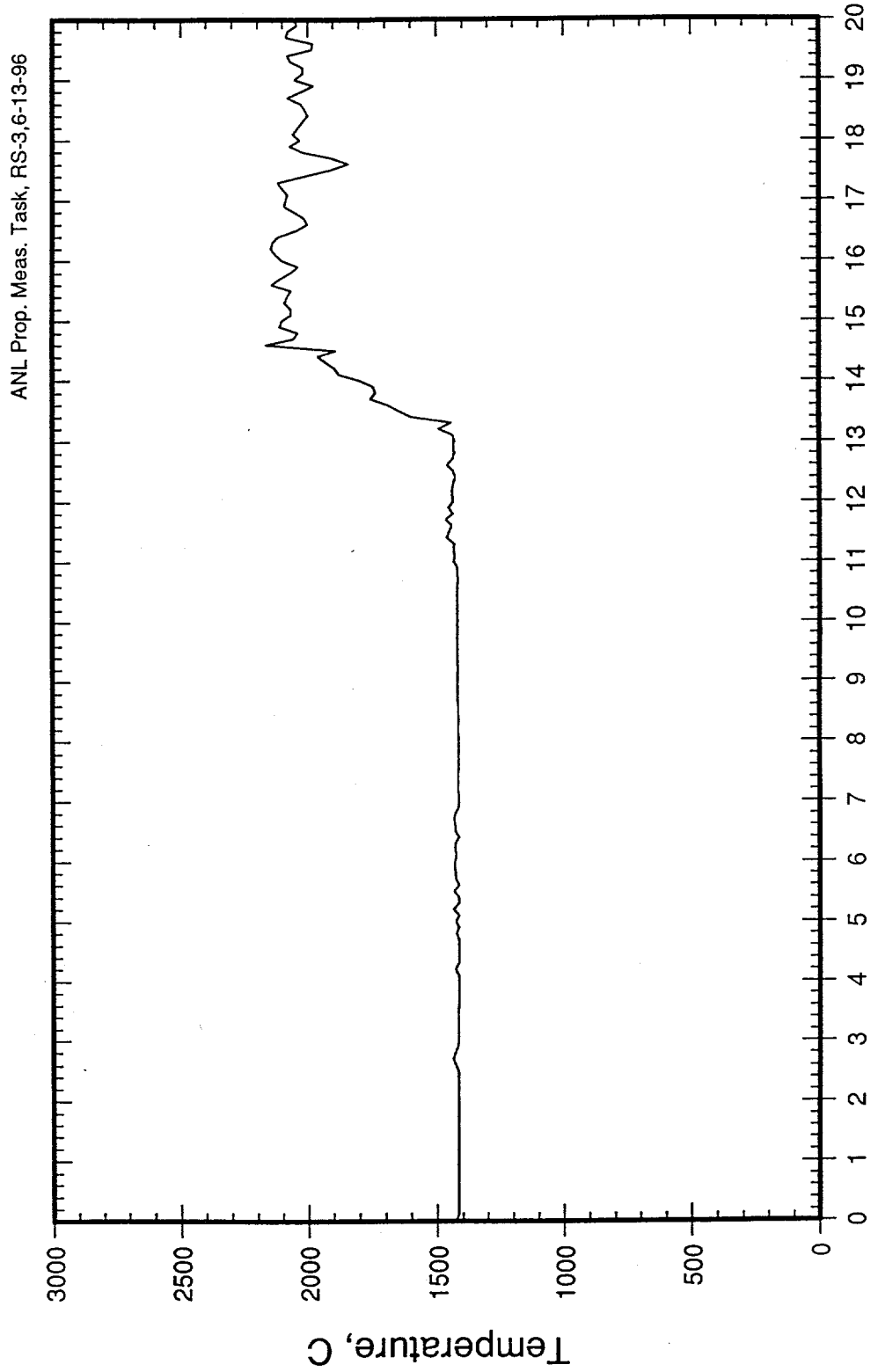

Figure 35. RS-3 Pyrometer Data

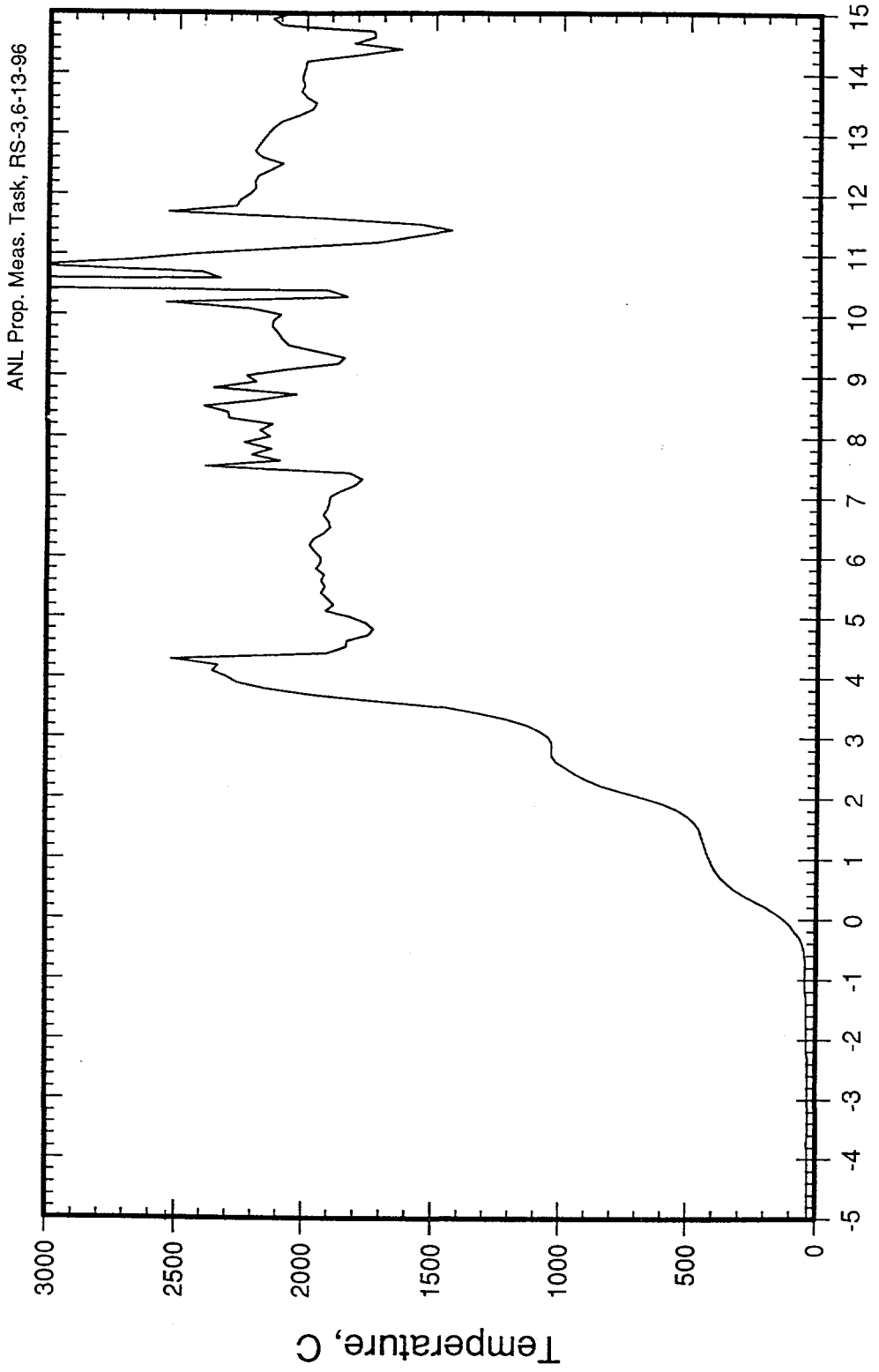

Figure 36. Melt Temperature 20.3 cm from Dam Location for RS-3

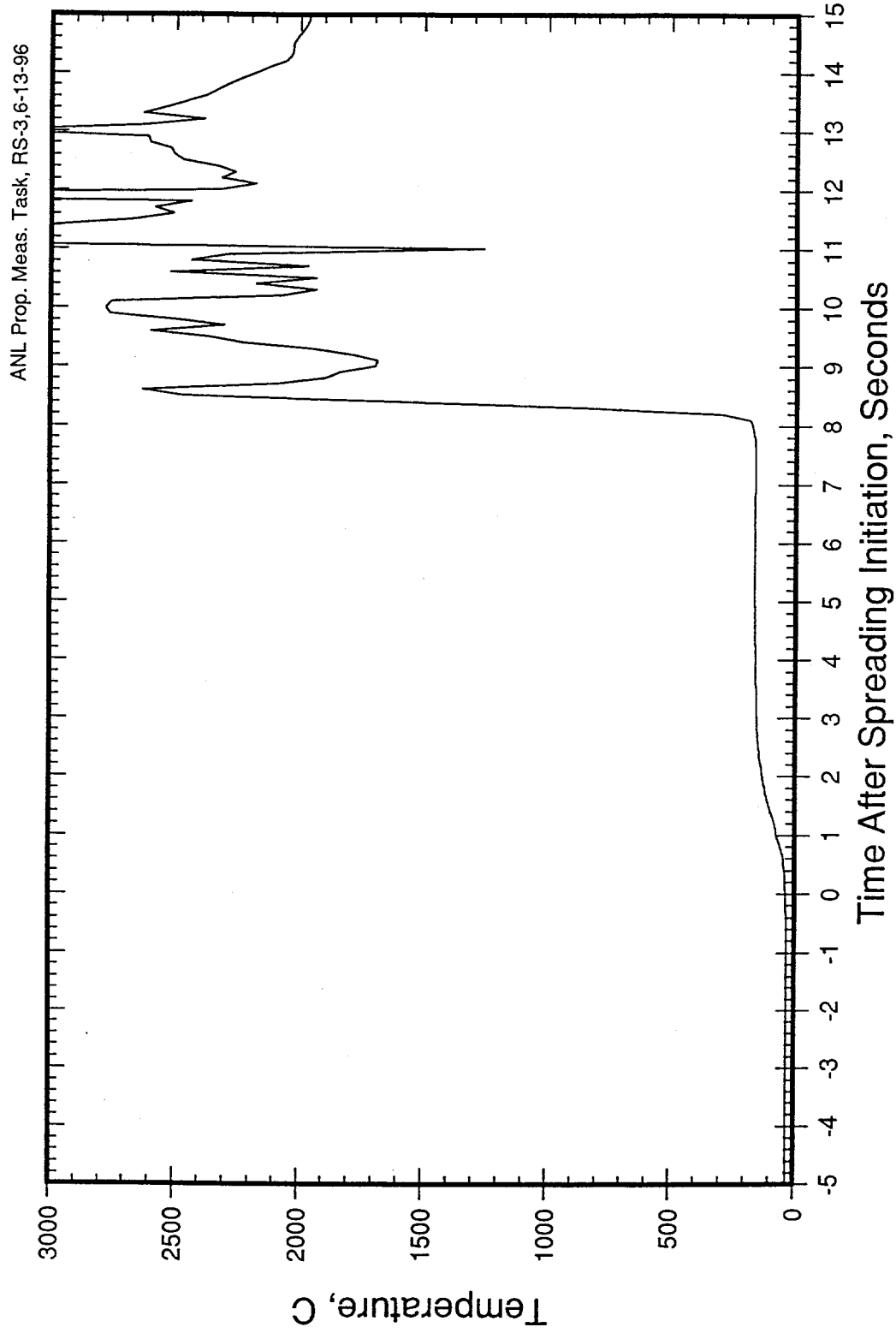

Figure 37. Melt Temperature 45.7 cm from Dam Location for RS-3

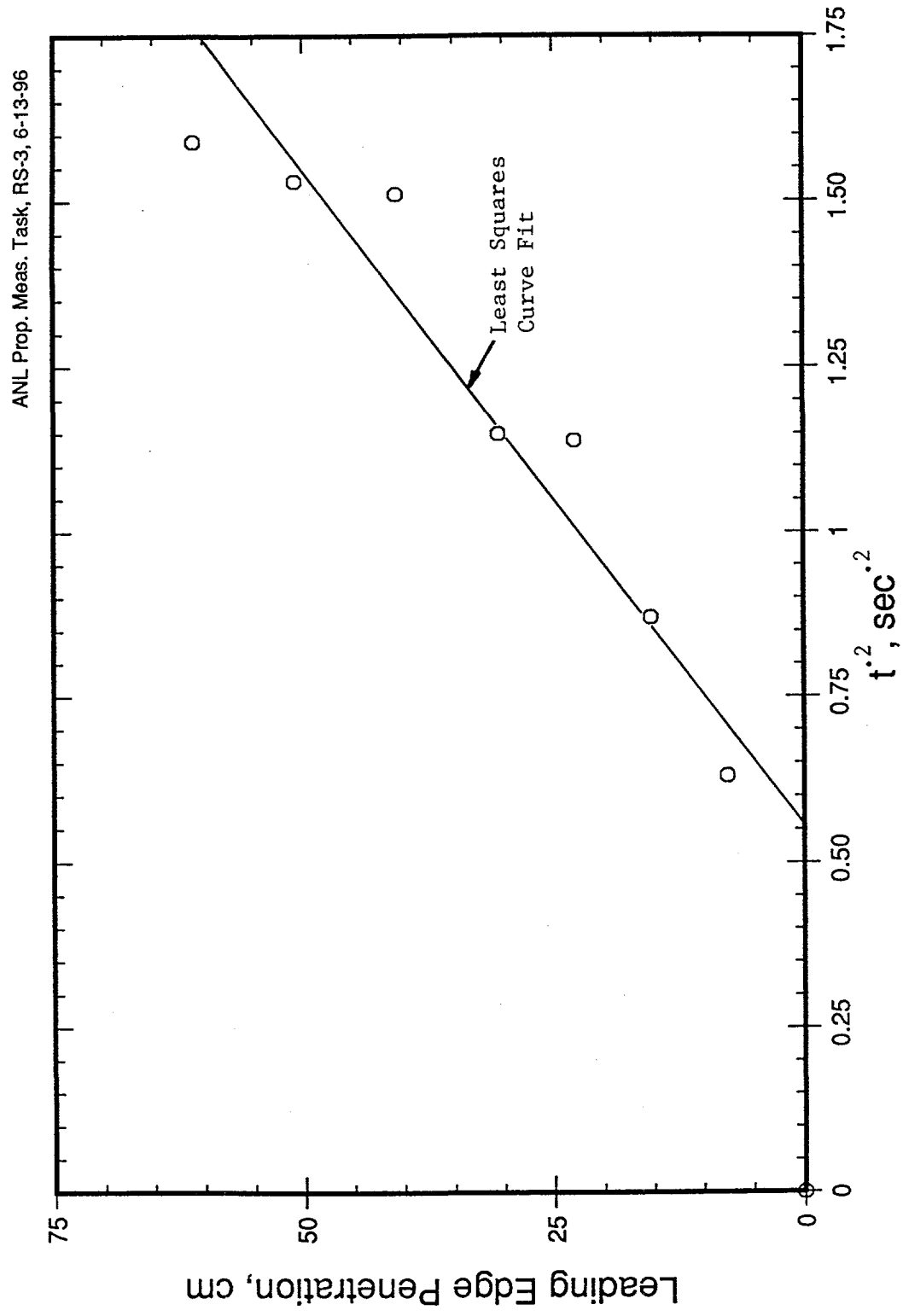

Figure 38. RS-3 Melt Leading Edge Location Versus $t^{1/5}$

order-of-magnitude estimate of the transition time be tween inertial and viscous-dominated spreading regimes is calculated to be 0.9 seconds for this test (see Eq. 2) given the best-estimate viscosity and other data described above. The estimated transition time is much less than the actual spreading of nominally 10 seconds. Thus, the spreading characteristics were clearly dominated by viscous effects for this experiment.

During posttest examinations, the solidified debris depth was measured as a function of spreading distance at the centerline of the channel. The data is provided in Figure 39 for spreading model validation purposes. The mass of Mo metal recovered from the melt generator region for test RS-2 is shown in Table 12. The recovered mass exceeds the theoretical Mo mass by 25% (see Table 15) which is attributable in part to the fact that the metal and oxide were partially bonded together at the interface, making separation of the two materials difficult during posttest disassembly.

Table 16 provides a summary comparison of the best-estimate melt temperature and calculated corium viscosity for all the tests. Also included in this table are the measured solidus and liquidus temperatures (see previous section) which were obtained with corium mixtures in which stainless steel was absent as an initial melt constituent. In addition, the estimated melt solid fraction for these three tests is shown in the table. These estimates were obtained from calculations performed with the OXY5-GEMINI2 Code[10]. Comparison of the data from tests RS-0, RS-2, and RS-3 indicates that corium viscosity increases as the zirconium oxidation level increases. For example, the viscosity is observed to increase by three orders of magnitude as the Zr oxidation increases from 30 to 70% at a constant temperature of nominally 2500 C. As is evident from the table, this trend may in part be due to buildup of solids in the melt, which is traceable to increasing liquidus temperature as the Zr oxidation increases. Comparison of the results from test RS-2 and RS-3 does not indicate any strong influence of stainless steel on the corium viscosity at this low oxidation level. However, the test with no stainless steel had an initial melt temperature which was ~ 170 C higher than the test in which stainless steel was present. Thus, the absence of any large variation in viscosity may in part be attributable to temperature differences between the two tests.

3.3 Recommendations for Additional Testing

The results of the initial test series indicates that the experiment approach for characterizing corium viscosity over a wide range of core oxidation states is viable. During this work, several

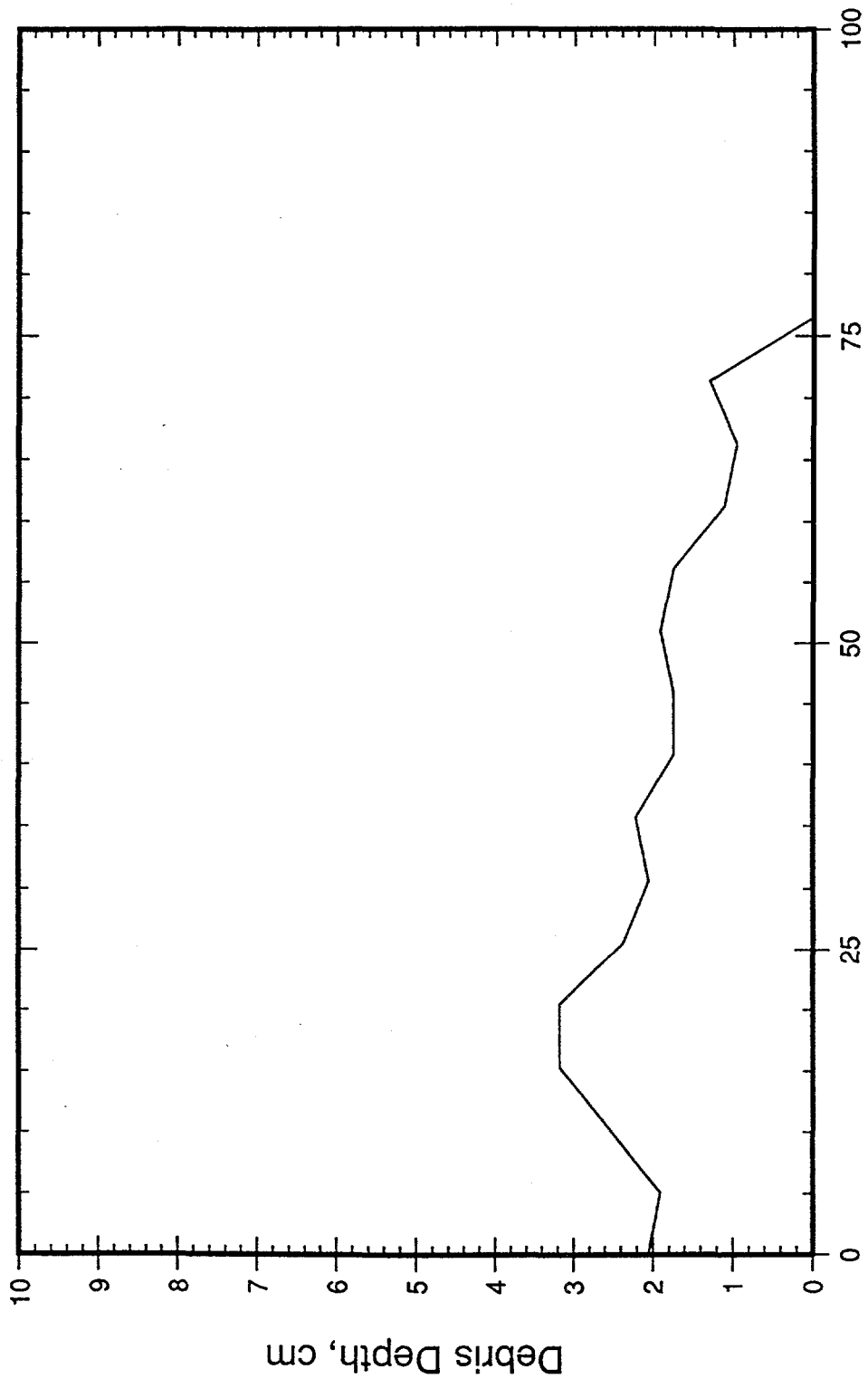

Figure 39. RS-3 Posttest Debris Configuration

Table 16. Corium Viscosity Determined from Spreading Data for Various Zr Oxidation Levels (Corium without SS)

Test No.	Zr Oxidation (%)	Corium Temperature (C)	Best Estimate Viscosity (cp)	Viscosity Error Range (cp)	Corium[1] Liquidus/Solidus (C/C)	Estimated[2] Melt Solid Fraction (-)
RS-2	30	2520	4.4	3.8-5.0	1950/2280	0
RS-0	50	2470	110	63-212	2000/2500	0.23
RS-3	70	2530	5070	2650-10700	2000/2600	0.40

1. Based on measurements with same corium compositions in DTA apparatus.

2. Based on code calculations by Thermodata; presented at ACE/TAC Meeting.

points were identified which would improve the experiment technique. These points are summarized as follows:

i) Improve the dam design. The dam design for initiating the spreading transient worked well in two tests, but shortcomings were identified in the other two experiments. Thus, the design should be reconsidered in order to improve the spreading initiation phase of the experiment. This will reduce uncertainties in the interpretation of the test data.

ii) Add additional, diverse instrumentation to provide independent estimates of the corium viscosity. For instance, the melt viscosity can also be estimated based on measurements of the local melt height versus time, as opposed to the leading edge penetration. It is recommended to develop a simple probe for measuring local melt depth to add diversity to the measurement techniques.

iii) Improve Type C (Melt Temperature) thermocouple design. In these tests, bare sheath Type C thermocouples were used to measure local melt temperature. In many instances, these TC's failed prior to reaching peak temperature. It is recommended to add a high thermal conductivity, low heat capacity, thermowell for these TC's to improve their survivability.

In addition to the above improvements in the experiment technique, it is important to conduct additional tests to expand the parameter ranges considered in this study. As described in the recommendations for the previous section, the corium compositions considered in this study are consistent with most US BWR core compositions. The UO_2/ZrO_2 ratio in the experiments should be expanded to include additional tests with PWR core compositions. In addition, the completed series of tests were conducted with an initial melt temperature of nominally 2500 C. Additional tests should be conducted which span the liquidus/solidus range for a given composition to obtain additional data on the effect of melt temperature (viz., solid fraction) on the viscosity.

ACKNOWLEDGMENTS

Support for this work was provided by the International Nuclear Safety Center (INSC) at Argonne. Technical input regarding the experiment approach for the corium liquidus/solidus temperature measurements was provided by Drs. Joanne K. Fink and Leonard Leibowitz at Argonne. Sample preparation and metallography for these tests was performed by Mr. John C. Cassulo and Dr. John W. Holland, respectively. The analytical chemistry work was performed by the Analytical Chemistry Lab (ACL) at Argonne. This effort was led by Dr. Don Graczyk. These efforts are gratefully acknowledged.

5.0 REFERENCES

1. M. I. Pope and M. D. Judd, Differential Thermal Analysis, Heyden & Sons Ltd. (1977).

2. H. E. Huppert, "The Propagation of Two-Dimensional and Axisymmetric Viscous Gravity Currents Over a Rigid Horizontal Surface," J. Fluid Mechs., Vol. 121, p. 43 (1982).

3. V. F. Strizhov, personal communication, Russian Academy of Science, Nuclear Safety Institute (November, 1995).

4. Omega Complete Temperature Measurement Handbook and Encyclopedia, Omega Engineering, Inc. (1995).

5. A. Skokan, "High Temperature Phase Relations in the U-Zr-O System," Fifth International. Meeting on Thermal Nuclear Reactor Safety, Karlsruhe, Germany, September 9-13, 1984, Vol. 2, p. 1035.

6. M. F. Roche, L. Leibowitz, J. K. Fink, and L. Baker, Jr., "Solidus and Liquidus Temperatures of Core-Concrete Mixtures," NUREG/CR-6032 (April 1993).

7. H. S. Mickley, T. K. Sherwood, and C. E. Reed, Applied Mathematics in Chemical Engineering, Second Edition, McGraw-Hill Book Company, Inc., New York, New York (1957).

8. J. L. Binder, L. M. McUmber, and B. W. Spencer, "Direct Containment Heating Integral Effects Tests at 1/40 Scale in Zion Nuclear Power Plant Geometry," NUREG/CR-6169, ANL-94/18 (September 1994).

9. J. K. Fink, M. G. Chansanov, and L. Leibowitz, "Thermophysical Properties of Uranium Dioxide," J. Nucl. Materials, Vol. 102, p. 17 (1981).

10. P. Y. Chevalier, "Presentation of the OXY5-GEMINI2 Code," presentation at Advanced Containment Experiments Technical Advisory Committee Meeting, Palo Alto, CA, November 4-8, 1991.